ESAIM: M2AN 51 (2017) 165–186
DOI: 10.1051/m2an/2016016

ESAIM: Mathematical Modelling and Numerical Analysis
www.esaim-m2an.org

SUPERCONVERGENCE BY M-DECOMPOSITIONS. PART II: CONSTRUCTION OF TWO-DIMENSIONAL FINITE ELEMENTS *

Bernardo Cockburn[1] and Guosheng Fu[1]

Abstract. We apply the concept of an M-decomposition introduced in Part I to systematically construct local spaces defining superconvergent hybridizable discontinuous Galerkin methods, and their companion sandwiching mixed methods. This is done in the framework of steady-state diffusion problems for the h- and p-versions of the methods for general polygonal meshes in two-space dimensions.

Mathematics Subject Classification. 65M60, 65N30, 58J32, 65N15.

Received September 29, 2015. Revised February 16, 2016. Accepted March 2nd, 2016.

1. Introduction

This is the second of a series of papers in which we develop the concept of an M-decomposition as an effective tool for devising hybridizable discontinuous Galerkin (HDG) methods, and their companion sandwiching mixed methods, which superconverge on unstructured meshes of shape-regular polyhedral elements. In the first part of this series, [20], the general theory of M-decompositions was developed in the frame of steady-state diffusion problems:

$$\begin{aligned} \mathrm{c}\boldsymbol{q} + \nabla u &= 0 && \text{in } \Omega, \\ \nabla \cdot \boldsymbol{q} &= f && \text{in } \Omega, \\ u &= g && \text{on } \partial\Omega, \end{aligned}$$

where $\Omega \subset \mathbb{R}^2$ is a bounded polygonal domain, c is a uniformly bounded, uniformly positive definite symmetric matrix-valued function, $f \in L^2(\Omega)$ and $g \in H^{1/2}(\partial\Omega)$. Here we apply it systematically to explicitly construct ready-for-implementation local spaces admitting M-decompositions for a variety of finite elements defined on general polygonal elements in two-space dimensions. The corresponding construction in three-space dimensions, which is fundamentally different than the two-dimensional case due to the difference in the characterization of divergence-free polynomials in $\mathbb{R}^2$ and $\mathbb{R}^3$, is carried out in Part III, [14], of this series.

To better describe our results, let us recall the definition of the HDG (and mixed) methods under consideration; we use the notation used in Part I, [20]. The HDG methods seek an approximation to $(u, \boldsymbol{q}, u|_{\mathcal{E}_h})$,

Keywords and phrases. Hybridizable discontinuous Galerkin methods, superconvergence, polygonal meshes.

* *The first author was partially supported by the National Science Foundation (Grant DMS-1115331).*

[1] School of Mathematics, University of Minnesota, Minneapolis, MN 55455, USA.
cockburn@math.umn.edu; fuxxx165@math.umn.edu

TABLE 1. Construction of spaces $\boldsymbol{V} \times W$ admitting an M-decomposition, where the space of traces $M(\partial K)$ includes the constants. The given space $\boldsymbol{V}_g \times W_g$ satisfies the inclusion properties (I). We assume that $W \supset \mathcal{P}_0$).

$\boldsymbol{V}$	W
$\boldsymbol{V}^{\mathrm{mix}} := \boldsymbol{V}_g \oplus \delta\boldsymbol{V}_{\mathrm{fillM}} \oplus \delta\boldsymbol{V}_{\mathrm{fillW}}$	$W^{\mathrm{mix}} := W_g$
$\boldsymbol{V}^{\mathrm{hdg}} := \boldsymbol{V}_g \oplus \delta\boldsymbol{V}_{\mathrm{fillM}}$	$W^{\mathrm{hdg}} := W_g$
$\boldsymbol{V}_{\mathrm{mix}} := \boldsymbol{V}_g \oplus \delta\boldsymbol{V}_{\mathrm{fillM}}$	$W_{\mathrm{mix}} := \nabla \cdot \boldsymbol{V}_g$

$(u_h, \boldsymbol{q}_h, \widehat{u}_h)$, in the finite element space $W_h \times \boldsymbol{V}_h \times M_h$, of the form

$$
\begin{aligned}
\boldsymbol{V}_h &:= \{\boldsymbol{v} \in \boldsymbol{L}^2(\mathcal{T}_h) : \boldsymbol{v}|_K \in \boldsymbol{V}(K),\ K \in \mathcal{T}_h\},\\
W_h &:= \{w \in L^2(\mathcal{T}_h) : w|_K \in W(K),\, K \in \mathcal{T}_h\},\\
M_h &:= \{\mu \in L^2(\mathcal{E}_h) :\ \mu|_F \in M(F),\ \ F \in \mathcal{E}_h\},
\end{aligned}
$$

which is determined as the only solution of the following weak formulation:

$$
\begin{aligned}
(\mathrm{c}\,\boldsymbol{q}_h\,,\,\boldsymbol{v})_{\mathcal{T}_h} - (u_h\,,\,\nabla\cdot\boldsymbol{v})_{\mathcal{T}_h} + \langle \widehat{u}_h\,,\,\boldsymbol{v}\cdot\boldsymbol{n}\rangle_{\partial\mathcal{T}_h} &= 0, && \text{(1.1a)}\\
-\,(\boldsymbol{q}_h\,,\,\nabla w)_{\mathcal{T}_h} + \langle \widehat{\boldsymbol{q}}_h\cdot\boldsymbol{n}\,,\,w\rangle_{\partial\mathcal{T}_h} &= (f\,,\,w)_{\mathcal{T}_h}, && \text{(1.1b)}\\
\langle \widehat{\boldsymbol{q}}_h\cdot\boldsymbol{n},\mu\rangle_{\partial\mathcal{T}_h\setminus\partial\Omega} &= 0, && \text{(1.1c)}\\
\langle \widehat{u}_h,\mu\rangle_{\partial\Omega} &= \langle g,\mu\rangle_{\partial\Omega}, && \text{(1.1d)}
\end{aligned}
$$

for all $(w, \boldsymbol{v}, \mu) \in W_h \times \boldsymbol{V}_h \times M_h$, where

$$
\widehat{\boldsymbol{q}}_h\cdot\boldsymbol{n} = \boldsymbol{q}_h\cdot\boldsymbol{n} + \alpha(u_h - \widehat{u}_h) \quad \text{ on } \quad \partial\mathcal{T}_h.
$$

In Part I, [20], it was shown that these methods are superconvergent on unstructured meshes if, for all elements $K \in \mathcal{T}_h$, the local space $\boldsymbol{V}(K) \times W(K)$ admits an $M(\partial K)$-decomposition, where

$$
M(\partial K) := \{\mu \in L^2(\partial K) :\ \mu|_e \in M(e) \text{ for all edges } e \text{ of } K\}.
$$

Moreover, it was also shown how to construct M-decompositions for any given space $M(\partial K)$.

We can summarize the construction as follows. (From now on, if there is no confusion, we drop the dependence of the local spaces on the element K.) Given the trace space M that contains constants on ∂K, we pick any *given* space $\boldsymbol{V}_g \times W_g$ satisfying the inclusion properties:

(I.1) $\gamma\boldsymbol{V}_g + \gamma W_g \subset M$,
(I.2) $\nabla W_g \times \nabla\cdot\boldsymbol{V}_g \subset \boldsymbol{V}_g \times W_g$,

where $\gamma\boldsymbol{V}_g := \{\boldsymbol{v}\cdot\boldsymbol{n}|_{\partial K}\ :\ \boldsymbol{v} \in \boldsymbol{V}_g\}$ and $\gamma W_g := \{w|_{\partial K}\ :\ w \in W_g\}$. We then construct the three spaces $\boldsymbol{V} \times W$ described in Tables 1 and 2; each of them admits an M-decomposition. In Table 1, the space $\boldsymbol{V}^{\mathrm{hdg}} \times W^{\mathrm{hdg}}$ is associated to an HDG method (note that we have $\nabla\cdot\boldsymbol{V}^{\mathrm{hdg}} \subsetneq W^{\mathrm{hdg}}$), while the *upper* sandwiching space $\boldsymbol{V}^{\mathrm{mix}} \times W^{\mathrm{mix}}$ and the *lower* space $\boldsymbol{V}_{\mathrm{mix}} \times W_{\mathrm{mix}}$ are associated to mixed methods (note that we have $\nabla\cdot\boldsymbol{V}^{\mathrm{mix}} = W^{\mathrm{mix}}$ and $\nabla\cdot\boldsymbol{V}_{\mathrm{mix}} = W_{\mathrm{mix}}$). In Table 2, the space $\boldsymbol{V}_{g_s} := \{\boldsymbol{v} \in \boldsymbol{V}_g\ :\ \nabla\cdot\boldsymbol{v} = 0\}$ (s stands for solenoidal) is the divergence-free subspace of $\boldsymbol{V}_g$.

Let us recall that the two integers in the last column of Table 2 are the M- and the S-indexes. They are defined as follows:

$$
\begin{aligned}
I_M(\boldsymbol{V}_g \times W_g) &:= \dim M - \dim\{\boldsymbol{v}\cdot\boldsymbol{n}|_{\partial K} : \boldsymbol{v} \in \boldsymbol{V}_g, \nabla\cdot\boldsymbol{v} = 0\} - \dim\{w|_{\partial K} : w \in W_g, \nabla w = 0\},\\
I_S(\boldsymbol{V}_g \times W_g) &:= \dim W_g - \dim \nabla\cdot\boldsymbol{V}_g.
\end{aligned}
$$

TABLE 2. The properties of the spaces $\delta\boldsymbol{V}$. Here $\boldsymbol{V}_{g_s} := \{\boldsymbol{v} \in \boldsymbol{V}_g : \nabla\cdot\boldsymbol{v} = 0\}$.

$\delta\boldsymbol{V}$	$\nabla\cdot\delta\boldsymbol{V}$	$\gamma\delta\boldsymbol{V}$	$\dim\delta\boldsymbol{V}$	
$\delta\boldsymbol{V}_{\text{fillM}}$	$\{0\}$	$\subset M, \cap\gamma\boldsymbol{V}_{g_s} = \{0\}$	$I_M(\boldsymbol{V}_g \times W_g)$	$(=\dim\gamma\delta\boldsymbol{V})$
$\delta\boldsymbol{V}_{\text{fillW}}$	$\subset W_g, \cap\nabla\cdot\boldsymbol{V}_g = \{0\}$	$\subset M$	$I_S(\boldsymbol{V}_g \times W_g)$	$(=\dim\nabla\cdot\delta\boldsymbol{V})$

TABLE 3. The indexes for $M := \mathcal{P}_k(\partial K)$ for different elements K.

$\boldsymbol{V}_g \times W_g := \boldsymbol{\mathcal{Q}}_k \times \mathcal{Q}_k \quad (k \geq 1)$		
Element	$I_M(\boldsymbol{V}_g \times W_g)$	$I_S(\boldsymbol{V}_g \times W_g)$
Rectangle	2	1
$\boldsymbol{V}_g \times W_g := \boldsymbol{\mathcal{P}}_k \times \mathcal{P}_k \quad (k \geq 0)$		
Element	$I_M(\boldsymbol{V}_g \times W_g)$	$I_S(\boldsymbol{V}_g \times W_g)$
Triangle	$\underset{(k\geq 0)}{0}$	$k+1$
Quadrilateral	$\underset{(k=0)}{1} \quad \underset{(k\geq 1)}{2}$	$k+1$
Pentagon	$\underset{(k=0)}{2} \quad \underset{(k=1)}{4} \quad \underset{(k\geq 2)}{5}$	$k+1$
Hexagon	$\underset{(k=0)}{3} \quad \underset{(k=1)}{6} \quad \underset{(k=2)}{8} \quad \underset{(k\geq 3)}{9}$	$k+1$
Polygon of ne edges	$(ne-3)(\theta+1) - \frac{1}{2}\theta(\theta-1)$, $\theta := \min\{k, ne-3\}$	$k+1$

Once we find spaces $\boldsymbol{V} \times W$ admitting M-decompositions, we need to check the conditions

(J.1) $\mathcal{P}_0(K) \subset \nabla\cdot\boldsymbol{V}$,
(J.2) $\mathcal{P}_1(K) \subset W$,

to guarantee that the spaces actually define a superconvergent method. Here by superconvergence, we mean that there exists a projection of the scalar function u onto the finite element space W_h, denoted as $\Pi\, u$, such that the projection error $\Pi\, u - u_h$ convergences to zero *faster* than the error $u - u_h$. It is then possible to define a scalar postprocessing u_h^* converging to u as fast as $\Pi u - u_h$.

Although the construction just sketched is independent of the space dimension, in this paper, we restrict ourselves to the two-dimensional case. We mainly focus on the construction of the spaces $\delta\boldsymbol{V}_{\text{fillM}}$ and $\delta\boldsymbol{V}_{\text{fillW}}$ on a general polygonal element K in two dimensions, which are *ready for implementation*, for the trace space

$$M := \mathcal{P}_k(\partial K) = \{\mu \in L^2(\partial K) : \ \mu|_e \in \mathcal{P}_k(e) \text{ for all edges } e \text{ of } K\},$$

and the given space $\boldsymbol{V}_g \times W_g := \boldsymbol{\mathcal{P}}_k(K) \times \mathcal{P}_k(K)$. Here $\mathcal{P}_k(D)$ denotes the space of polynomials of degree at most k defined on a domain D. When the element K is a unit square, we also consider the tensor-product given space $\boldsymbol{V}_g \times W_g := \boldsymbol{\mathcal{Q}}_k(K) \times \mathcal{Q}_k(K)$. As mentioned above, the construction of the corresponding spaces on polyhedral elements is carried out in Part III, [14]. The reason we need to do this elsewhere is that the construction of the space $\delta\boldsymbol{V}_{\text{fillM}}$, which is the most difficult part of the construction, relies on a characterization of the divergence-free space $\{\boldsymbol{v} \in \boldsymbol{V}_g : \nabla\cdot\boldsymbol{v} = 0\}$ and that of the space of its normal traces. Such characterizations are *significantly* more involved in the three-dimensional case.

A glance at Table 2 is enough to make us realize that the spaces $\delta\boldsymbol{V}_{\text{fillM}}$ and $\delta\boldsymbol{V}_{\text{fillW}}$ are not unique on a given polygonal element K for given spaces $\boldsymbol{V}_g \times W_g$ and M; see also ([20], Props. 5.1 and 5.3). On the other hand, the dimensions of the spaces $\delta\boldsymbol{V}_{\text{fillM}}$ and $\delta\boldsymbol{V}_{\text{fillW}}$, that is, $I_M(\boldsymbol{V}_g \times W_g)$ and $I_S(\boldsymbol{V}_g \times W_g)$, respectively, are actually unique, as we see in Table 3. Indeed, recall that $I_M(\boldsymbol{V}_g \times W_g)$ is the smallest dimension of a space $\delta\boldsymbol{V}_{\text{fillM}}$ such that $\boldsymbol{V} \times W := \boldsymbol{V}_g \oplus \delta\boldsymbol{V}_{\text{fillM}} \times W_g$ admits an M-decomposition, see remark after ([20], Prop. 5.1), and that $I_S(\boldsymbol{V}_g \times W_g)$ is the smallest dimension of a space $\delta\boldsymbol{V}_{\text{fillW}}$ such that $\boldsymbol{V} \times W := \boldsymbol{V}_g \oplus \delta\boldsymbol{V}_{\text{fillM}} \oplus \delta\boldsymbol{V}_{\text{fillW}} \times W_g$ admits an M-decomposition with $\nabla \cdot \boldsymbol{V} = W$, see remark after ([20], Prop. 5.3). Moreover, from Table 3 for the case $\boldsymbol{V}_g \times W_g := \boldsymbol{\mathcal{P}}_k \times \mathcal{P}_k$, we notice that the S-index, $I_S(\boldsymbol{V}_g \times W_g)$, only depends on the polynomial degree k, not on the geometry of the element. In contrast, the M-index, $I_M(\boldsymbol{V}_g \times W_g)$, does depend on both the polynomial degree k and on the number of edges, ne, of the polygonal element. In particular, $k \mapsto I_M(\boldsymbol{V}_g \times W_g)$ is an increasing function on k for $k \leq ne-3$, and is equal to $\frac{1}{2}ne(ne-3)$ for any $k \geq ne-3$.

Let us briefly discuss how do we actually carry out the construction of the spaces $\boldsymbol{V} \times W$ admitting M-decompositions. The main idea is to find a basis for a complement in the space of (non-constant) traces in $M(\partial K)$ of the normal traces of $\boldsymbol{V}_g$. Once this basis is found, the space $\delta\boldsymbol{V}_{\text{fillM}}$ is obtained as the span of a *lifting* of each of the traces into the element K. To find a basis of the above-mentioned complement, we proceed by induction on the edges of the polygonal element K. This allows us to consider spaces of traces defined on a single edge at a time and results in a systematic way to dealing with any polygonal element. The price we must pay is that the resulting space $\delta\boldsymbol{V}_{\text{fillM}}$ will depend on the numbering of the edges of the elements. However, as shown in [20], this does not affect the superconvergence properties of the associated method. Moreover, when symmetries are needed, it is not difficult to modify our results to get the symmetry-satisfying spaces.

Note that the HDG methods we obtain by our construction are strongly related to mixed methods, as the *sandwiching* methods displayed the first and last rows of Table 1 are associated to (hybridized versions of) mixed methods. Because of this, we can consider that our approach is the first systematic, constructive way of obtaining mixed methods for polynomial elements of arbitrary shape. Indeed, although the theory of mixed methods has been well-explored since the seminal paper of Raviart and Thomas back in 1977 [31], most mixed methods for diffusion problems in two dimensions are available for meshes made of triangular or square elements *only*, see [6]. In fact, to the knowledge of the authors, the only element for which high-order mixed elements were defined is a convex quadrilateral, see [2]; the spaces provided by our construction are smaller and provide similar convergence properties. Mixed methods of lowest order ($k = 0$) on polygonal/polyhedral meshes have been proposed in [26, 27], where the authors use composite piecewise linear functions to define the $H(\text{div})$-conforming space; see also in [32] where a different lowest order composite mixed method on general hexahedral meshes was introduced. High-order mixed methods on polygonal meshes has been considered in ([33], Sect. 7). However, this method is actually a reformulation of a standard mixed method on a *matching simplicial submesh* of the original polygonal mesh, see ([33], Thm. 7.2). It is unclear whether this kind of reformulation would be more efficient to implement than the original mixed method on the matching simplicial submesh.

Let us now briefly contrast our mixed methods with the mixed virtual element methods on two-dimensional polygonal meshes in [9]; for the three-dimensional case, see [5]. The spaces used by these methods, on each element, use solutions to certain PDEs as basis functions. As for the original conforming virtual element methods, [4], since the basis functions themselves are not computable, a set of degrees of freedom that can be used to *exactly* compute volume integrals related to the polynomial parts of the basis functions has to be identified. Then some integrals must be replaced by a suitably chosen "stabilization" term so that the method keeps its original high-order accuracy. In contrast, our high-order $H(\text{div})$-conforming spaces are obtained by adding to $\boldsymbol{V}_g$ a small number of explictly computable basis functions. Indeed, as pointed out above, for $\boldsymbol{V}_g \times W_g := \boldsymbol{\mathcal{P}}_k \times \mathcal{P}_k$, the dimension of $\delta\boldsymbol{V}_{\text{fillM}}$ is at most $\frac{1}{2}\,ne\,(ne-3)$ and that of $\delta\boldsymbol{V}_{\text{fillW}}$ is $k+1$.

Let us now compare of our methods against other HDG methods that achieve superconvergence without using M-decompositions. Currently, there are two ways of devising superconvergent HDG methods without relying on M-decompositions. One uses a new stabilization operator suggested back in 2010 in ([28], Rem. 1.2.4) by Lehrenfeld–Schöberl projection. A complete error analysis of these superconvergent HDG methods (defined on general polygonal of polyhedral elements) was performed by Oikawa recently in [30]. Another way consists in defining a sophisticated numerical trace for the approximate flux. This definition is the distinctive feature of the so-called hybrid high-order (HHO) methods introduced in [22, 23] which superconverge also for polygonal or polyhedral elements of arbitrary shape. It can be easily incorporated into the family of HDG methods since HHO methods can be rewritten as HDG methods, as shown in [21]; see [13] for the different ways of rewriting

HDG methods. One advantage of these these methods over the spaces we provide is that they do display *smaller* local spaces. On the other hand, for the same space $M(\partial K)$, both these methods and ours have a global matrix equation of identical size and sparsity structure. Thus, it is reasonable to expect that, if the computation of the local problems is done in parallel, the main computational effort of all of these methods should be essentially the same. Our numerical results in Section 5 shows that, on a polygonal mesh, all these methods produce similar results in terms of numerical error and computational cost.

Let us end by pointing out that, by using our results for the sandwiching mixed methods, we can locally compute an $H(\mathrm{div})$-conforming flux postprocessing, see ([20], Sect. 6.3), for the HDG approximation. This also applies to the other methods like the HDG with the LS stabilization function or the HHO methods. This postprocessing can be thought of as a generalization of the postprocessing obtained back in 2003 by Bastian and Rivière [3] (see the variations proposed, for simplicial meshes, in 2005 [16], in 2007 [24] and in 2010 in [18]). As was argued therein, see also ([1], Sect. 2.2), $H(\mathrm{div})$-conforming fluxes obtained by postprocessing an DG-like approximate flux are preferable to the original DG-like approximation, even if both approximations are of the same accuracy, when used on other convection-diffusion problems in which these fluxes drive the convection.

The rest of the paper is organized as follows. In Section 2, we describe and discuss our constructions of M-decompositions. In Section 3, we provide the proofs of all the results of Section 2. In Section 4, we extend our results to elements with hanging nodes (which may be useful in h-adaptivity), and to the variable-degree case in which

$$M(\partial K) := \{\mu \in L^2(\partial K) :\ \mu|_e \in \mathcal{P}_{k_e}(e) \text{ for all edges } e \text{ of } K\},$$

and $k_e \geq 0$ can vary from edge to edge (which may be useful in p-adaptivity). Then, in Section 5, we provide numerical results to compare with some other HDG methods, and illustrate the superconvergence properties of the new (uniform-degree) HDG methods and their sandwiching mixed methods on polygonal meshes. We end in Section 6 with some concluding remarks.

2. The main results

This section contains our main results, that is, the spaces $\delta\boldsymbol{V}_{\mathrm{fillM}}$ and $\delta\boldsymbol{V}_{\mathrm{fillW}}$ satisfying the properties in Table 2. We consider the two above-mentioned choices of the initial guess spaces $\boldsymbol{V}_g \times W_g$ and general polygonal elements. Here, we use the following notation:

$$\mathbf{curl}\, p := (-p_y, p_x).$$

2.1. The case $\boldsymbol{V_g} \times \boldsymbol{W_g} := \boldsymbol{\mathcal{Q}_k} \times \boldsymbol{\mathcal{Q}_k}, \boldsymbol{k} \geq \mathbf{1}$

In this case, we obtain mostly already known methods which we can see under a different light.

Theorem 2.1. *Let K be the unit square with edges parallel to the axes. Then, for $M = \mathcal{P}_k(\partial K)$ and $\boldsymbol{V}_g \times W_g = \boldsymbol{\mathcal{Q}}_k(K) \times \mathcal{Q}_k(K)$, where $k \geq 1$, we have that*

$$I_M(\boldsymbol{V}_g \times W_g) = 2 \quad \text{and} \quad I_S(\boldsymbol{V}_g \times W_g) = 1.$$

Moreover, the space

$$\delta\boldsymbol{V}_{\mathrm{fillM}} := \mathbf{curl}\ \mathrm{span}\{x^{k+1}y, x\, y^{k+1}\},$$
$$\delta\boldsymbol{V}_{\mathrm{fillW}} := \mathrm{span}\{(x^{k+1}y^k, x^k y^{k+1})\}.$$

satisfy the properties in Table 2.

The proof of this result is quite simple, hence omitted.

In addition to properties in Table 2, the spaces in Theorem 2.1 consists of polynomials that are invariant under the coordinate permutation $(x, y) \longrightarrow (y, x)$, hence they are easy to implement and preserve the symmetry

TABLE 4. A construction for K a square, $M = \mathcal{P}_k(\partial K)$ and $\boldsymbol{V}_g \times W_g = \boldsymbol{\mathcal{Q}}_k \times \mathcal{Q}_k$, $k \geq 1$.

$\boldsymbol{V}(K)$	$W(K)$	Method
$\boldsymbol{\mathcal{Q}}_k \oplus \mathbf{curl}\,\mathrm{span}\{x^{k+1}y, x\,y^{k+1}\} \oplus \mathrm{span}\{(x^{k+1}y^k, x^k y^{k+1})\}$	$\mathcal{Q}_k$	$\mathbf{TNT}_{[k]}$ [15,19]
$\boldsymbol{\mathcal{Q}}_k \oplus \mathbf{curl}\,\mathrm{span}\{x^{k+1}y, x\,y^{k+1}\}$	$\mathcal{Q}_k$	$\mathbf{HDG}^{Q}_{[k]}$ [19]
$\boldsymbol{\mathcal{Q}}_k \oplus \mathbf{curl}\,\mathrm{span}\{x^{k+1}y, x\,y^{k+1}\}$	$\mathcal{Q}_k \setminus \{x^k\,y^k\}$	new

of the square element K. The local spaces $\boldsymbol{V} \times W$ resulting from this result (see Tab. 1) are displayed in Table 4, where we abuse the notation and write $\mathcal{Q}_k \setminus \{x^k\,y^k\}$ instead of $\nabla \cdot \boldsymbol{\mathcal{Q}}_k = \mathcal{P}_{k-1,k} + \mathcal{P}_{k,k-1}$. These three spaces satisfy the conditions (J) in the introduction for superconvergence. As a consequence, the approximations $\boldsymbol{q}_h, u_h$ converge with the optimal order of $k+1$ and the postprocessing u_h^* with order $k+2$. This is also the case for the well-known Raviart−Thomas space

$$\boldsymbol{V} := \mathcal{P}_{k+1,k} \times \mathcal{P}_{k,k+1} \quad \text{and} \quad W := \mathcal{Q}_k,$$

even though its approximate flux space strictly contains the corresponding space of $\mathbf{TNT}_{[k]}$, whose dimension is bigger by $2k-1$. Here $\mathcal{P}_{m,n} := \mathcal{P}_m(x) \otimes \mathcal{P}_n(y)$ is the tensor product space of variable degree.

2.2. The case $\boldsymbol{V}_g \times W_g := \boldsymbol{\mathcal{P}}_k \times \mathcal{P}_k, k \geq 0$

For this case, we present two different approaches depending on what type of function is used to construct the spaces we seek. In the first approach, we use polynomials. Unfortunately, this approach only works for triangles and parallelograms. This prompts the second approach, which is based on special *lifting* functions from the boundary of the element into its interior.

a. First approach: Polynomial functions

Triangles

Let us begin by considering triangular elements. We recover a very well-known result.

Theorem 2.2. *Let K be a triangle. Then, for $M := \mathcal{P}_k(\partial K)$ and $\boldsymbol{V}_g \times W_g = \boldsymbol{\mathcal{P}}_k(K) \times \mathcal{P}_k(K)$, we have that*

$$I_M(\boldsymbol{V}_g \times W_g) = 0 \quad \textit{and} \quad I_S(\boldsymbol{V}_g \times W_g) = k+1.$$

Moreover, the spaces

$$\delta \boldsymbol{V}_{\mathrm{fillM}} := \{\mathbf{0}\},$$
$$\delta \boldsymbol{V}_{\mathrm{fillW}} := \boldsymbol{x}\,\widetilde{\mathcal{P}}_k,$$

satisfy the properties in Table 2.

The proof of this result is very simple, hence omitted.

The local spaces $\boldsymbol{V} \times W$ resulting from this result are displayed in Table 5. The first two spaces are well-defined for $k \geq 0$ while the last for $k \geq 1$. The first two spaces satisfy the conditions (J) for superconvergence when $k \geq 1$, and the last when $k \geq 2$. For these cases, the postprocessing u_h^* converges with order $k+2$ for these three choices of local spaces.

TABLE 5. A construction for K a triangle, $M = \mathcal{P}_k(\partial K)$ and $\boldsymbol{V}_g \times W_g = \boldsymbol{\mathcal{P}}_k \times \mathcal{P}_k$.

	$\boldsymbol{V}(K)$	$W(K)$	Method
$k \geq 0$	$\boldsymbol{\mathcal{P}}_k \oplus \boldsymbol{x}\,\widetilde{\mathcal{P}}_k$	$\mathcal{P}_k$	$\mathbf{RT}_k$ [31]
$k \geq 0$	$\boldsymbol{\mathcal{P}}_k$	$\mathcal{P}_k$	$\mathbf{HDG}_k$[19]
$k \geq 1$	$\boldsymbol{\mathcal{P}}_k$	$\mathcal{P}_{k-1}$	$\mathbf{BDM}_k$ [7]

TABLE 6. The case $M = \mathcal{P}_k(\partial K), \boldsymbol{V}_g \times W_g = \boldsymbol{\mathcal{P}}_k \times \mathcal{P}_k$, and K is the unit square.

	$\boldsymbol{V}(K)$	$W(K)$	Method
$k \geq 0$	$\boldsymbol{\mathcal{P}}_k \oplus \mathbf{curl}\ \mathrm{span}\{x^{k+1}y, x\,y^{k+1}\} \oplus\ \boldsymbol{x}\,\widetilde{\mathcal{P}}_k(K)$	$\mathcal{P}_k$	(new)
$k \geq 0$	$\boldsymbol{\mathcal{P}}_k \oplus \mathbf{curl}\ \mathrm{span}\{x^{k+1}y, x\,y^{k+1}\}$	$\mathcal{P}_k$	(new)
$k \geq 1$	$\boldsymbol{\mathcal{P}}_k \oplus \mathbf{curl}\ \mathrm{span}\{x^{k+1}y, x\,y^{k+1}\}$	$\mathcal{P}_{k-1}$	$\mathbf{BDM}_{[k]}$ [7]

Parallelograms

Here we consider the case in which the element is a parallelogram. We only need to take the element K to be the unit square as the general case is readily obtained by a linear transformation.

Theorem 2.3. *Let K be the unit square. Then, for $M := \mathcal{P}_k(\partial K)$ and $\boldsymbol{V}_g \times W_g = \boldsymbol{\mathcal{P}}_k(K) \times \mathcal{P}_k(K)$, we have that*

$$I_M(\boldsymbol{V}_g \times W_g) = \begin{cases} 1 & \text{if } k = 0, \\ 2 & \text{if } k \geq 1. \end{cases} \qquad \text{and} \qquad I_S(\boldsymbol{V}_g \times W_g) = k+1.$$

Moreover, the space

$$\delta\boldsymbol{V}_{\mathrm{fillM}} := \mathbf{curl}\ \mathrm{span}\{x^{k+1}y, xy^{k+1}\},$$
$$\delta\boldsymbol{V}_{\mathrm{fillW}} := \boldsymbol{x}\,\widetilde{\mathcal{P}}_k(K),$$

satisfy the properties in Table 2.

Again, the proof of this result is very simple, hence omitted. Note that for $k=0$, $\delta\boldsymbol{V}_{\mathrm{fillM}} = \mathrm{span}\{(-y,x)\}$ has dimension 1.

The local spaces $\boldsymbol{V} \times W$ resulting form this result are displayed in Table 6. Note that the local space $\boldsymbol{V}^{\mathrm{hdg}} \times W^{\mathrm{hdg}}$ is strictly included in the space called $\mathbf{HDG}^P_{[k]}$ in [19], namely,

$$\boldsymbol{\mathcal{P}}_k \oplus \mathbf{curl}\ (x\,y\,\widetilde{\mathcal{P}}_k) \times \mathcal{P}_k.$$

This space admits an M-decomposition and its dimension is bigger than that of the space $\boldsymbol{V}^{\mathrm{hdg}} \times W^{\mathrm{hdg}}$ by $k-1$. Also, note that the space $\mathbf{BDFM}_{[k]}$ [8], namely,

$$\boldsymbol{V} \times W := \big(\mathcal{P}_{k+1} \setminus \{y^{k+1}\} \times \mathcal{P}_{k+1} \setminus \{x^{k+1}\}\big) \times \mathcal{P}_k,$$

admits an M-decomposition and that its dimension is bigger than that of the corresponding space in the first row of Table 6 by $k-1$. These five spaces satisfy the conditions (J) for superconvergence when $k \geq 1$, except for the space $\mathbf{BDM}_{[k]}$ which satisfies them when $k \geq 2$. In these circumstances, the approximations $\boldsymbol{q}_h, u_h$ converge with the optimal order of $k+1$ and the postprocessing u_h^* with order $k+2$.

Polygonal elements

Unfortunately, it turns out that it is not possible to carry out the construction of the spaces under consideration by using only polynomials for more general elements K, as we see in the next result, whose proof will be given in Section 3.

Theorem 2.4. *Let K be a polygon which is not a triangle or parallelogram. If $\boldsymbol{V}\times W$ admits an M-decompositon with $M := \mathcal{P}_k(\partial K)$ for some $k \geq 0$, and $\mathcal{P}_0 \subset W$, then $\boldsymbol{V}$ can not be solely polynomials.*

This result immediately shows that it is not possible to construct $\delta \boldsymbol{V}_{\mathrm{fillM}}$ satisfying the properties in Table 2 by solely using polynomials for a polygon that is not a triangle or a parallelogram. This impossibility prompts the need to take a different approach.

b. Second approach: Non-polynomial liftings

To state our result, we need to introduce some notation. Let $\{\mathbf{v}_i\}_{i=1}^{ne}$ be the set of vertices of the polygonal element K which we take to be counter-clockwise ordered. Let $\{\mathbf{e}_i\}_{i=1}^{ne}$ be the set of edges of K where the edge $\mathbf{e}_i$ connects the vertices $\mathbf{v}_i$ and $\mathbf{v}_{i+1}$. Here the subindexes are integers module ne, for example, $\mathbf{v}_{ne+1} = \mathbf{v}_1$. An illustration for a quadrilateral element K is presented in Figure 1. We also define, for $1 \leq i \leq ne$, λ_i to be the linear function that vanishes on edge $\mathbf{e}_i$ and equals to 1 at the node $\mathbf{v}_{i+1}$.

Now, we introduce functions which we are going to use as tools for *lifting* traces on ∂K inside the element K. To each vertex $\mathbf{v}_i$, $i = 1, \ldots, ne$, we associate a function $\xi_i \in H^1(K)$ satisfying the following conditions:

(L.1) $\xi_i|_{\mathbf{e}_j} \in \mathcal{P}_1(\mathbf{e}_j),\ j = 1, \ldots, ne,$
(L.2) $\xi_i(\mathbf{v}_j) = \delta_{i,j},\ j = 1, \ldots, ne,$

where $\delta_{i,j}$ is the Kronecker delta. Note that conditions (L.2) and (L.3) together ensure that the trace of ξ_i on the edges is only non-zero at $\mathbf{e}_{i-1}$ and $\mathbf{e}_i$, where they are linear. Next, we give examples of these functions.

(1) *Polynomial liftings.* For a triangle, the polynomial lifting $\xi_i^p := \lambda_{i+1}$ satisfies the conditions (L). For a parallelogram, the polynomials $\xi_i^p := \lambda_{i+1}\lambda_{i+2}$ satisfy the conditions (L). However, for general quadrilaterals, and for arbitrary polygonals, there are no such polynomial liftings.
(2) *Composite liftings.* Here, we present the first non-polynomial lifting with a composite function. Given a polygonal element K, we subdivde it into a set of triangles $K = \cup_{i=1}^{nt} T_i$ with nt being the total number of triangles. We denote the collection of vertices of these triangles by $\{\mathbf{v}_i\}_{i=1}^{nv}$ where nv is the number of total vertices of the subdivision $\{T_i\}_{i=1}^{nt}$ and $\{\mathbf{v}_i\}_{i=1}^{ne}$ is the collection of vertices of the polygon K. Then, we take ξ_i^c to be the piecewise linear function such that $\xi_i^c|_{T_i} \in \mathcal{P}_1(T_i)$ for $i = 1, \ldots, nt$, and $\xi_i^c(\mathbf{v}_j) = \delta_{i,j}$ for $j = 1, \ldots, nv$. It is trivial to verify that ξ_i^c satisfy the conditions (L).
If the element K is a convex polygon with ne edges, we can subdivide it into $ne-2$ triangles with T_i having vertices $\mathbf{v}_1, \mathbf{v}_i$, and $\mathbf{v}_{i+1}$ for $2 \leq i \leq ne-1$. Then, the number of vertices of the subdivision $\{T_i\}_{i=1}^{nt}$ is ne.

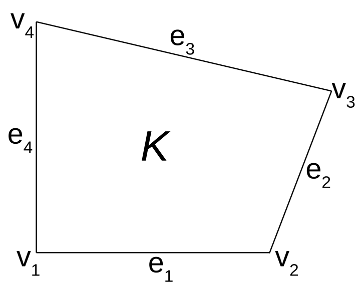

FIGURE 1. A quadrilateral element K.

If the element K is a start-shaped (not necessarily convex) polygon with respect to an interior node denoted as $\mathbf{v}_{ne+1}$, we can subdivde it into ne triangles with T_i having vertices $\mathbf{v}_i, \mathbf{v}_{i+1}$, and $\mathbf{v}_{ne+1}$ for $1 \le i \le ne-1$, and T_{ne} having vertices $\mathbf{v}_{ne}, \mathbf{v}_1$, and $\mathbf{v}_{ne+1}$. Then, the number of vertices of the subdivision $\{T_i\}_{i=1}^{nt}$ is $ne+1$. In our numerical examples in Section 5, we use the second choice of the subdivision with the node $\mathbf{v}_{ne+1}$ being the center of the polygon K. Numerical integration on K of these lifting functions can be easily performed by using standard quadrature rules for polynomials on each of the triangles T_i.

(3) *Generalized barycentric coordinates liftings.* A set of *generalized barycentric coordinates* (GBC) see [25,29,34] for the element K also satisfy conditions (L). In addition, they need to satisfy the partion of unity property $\sum_{i=1}^{ne} \xi_i = 1$, and the linear precision property $\sum_{i=1}^{ne} \mathbf{v}_i\, \xi_i(\boldsymbol{x}) = \boldsymbol{x}$. Although we do not require these two additional constrains, we can use any set of GBC to define our liftings.

We are now ready to state our construction. The proof of this result is quite complicated, and is postponed to Section 3.

Theorem 2.5. *Let K be a polygonal of ne edges such that no edges lie on the same line. Then, for $M := \mathcal{P}_k(\partial K)$ and $\boldsymbol{V}_g \times W_g = \boldsymbol{\mathcal{P}}_k(K) \times \mathcal{P}_k(K)$, we have that*

$$I_M(\boldsymbol{V}_g \times W_g) = (ne-3)(\theta+1) - \frac{1}{2}\theta(\theta-1), \qquad \text{and} \qquad I_S(\boldsymbol{V}_g \times W_g) = k+1,$$

here $\theta := \min\{k, ne-3\}$. Moreover, the spaces

$$\begin{aligned} \delta \boldsymbol{V}_{\text{fillM}} &:= \oplus_{i=1}^{ne} \mathbf{curl}\, \Psi_i, \\ \delta \boldsymbol{V}_{\text{fillW}} &:= \boldsymbol{x}\, \widetilde{\mathcal{P}}_k, \end{aligned}$$

satisfy the properties in Table 2. Here

$$\Psi_i = \begin{cases} \{0\} & \text{if} \quad i = 1,2, \\ \operatorname{span}\{\xi_{i+1}\lambda_{i+1}^b ; \max\{k+3-i, 0\} \le b \le k\} & \text{if} \quad 3 \le i \le ne-1, \\ \operatorname{span}\{\xi_{i+1}\lambda_{i+1}^b ; \max\{k+4-i, 1\} \le b \le k\} & \text{if} \quad i = ne. \end{cases}$$

Here, the functions $\{\xi_i\}_{i=1}^{ne}$ are liftings functions that satisfy conditions (L).

The local spaces $\boldsymbol{V} \times W$ resulting from this result are displayed in Table 7. The first two spaces are well-defined for $k \ge 0$, while the last for $k \ge 1$. The first two spaces satisfy the conditions (J) for superconvergence when $k \ge 1$, and the last when $k \ge 2$. For these cases, the postprocessing u_h^* converges with order $k+2$ for these three choices of local spaces.

TABLE 7. A construction for K a polygon without hanging nodes, $M = \mathcal{P}_k(\partial K)$ and $\boldsymbol{V}_g \times W_g = \boldsymbol{\mathcal{P}}_k \times \mathcal{P}_k$.

	$\boldsymbol{V}(K)$	$W(K)$
$(k \ge 0)$	$\boldsymbol{\mathcal{P}}_k \oplus_{i=1}^{ne} \mathbf{curl}\, \Psi_i \oplus \boldsymbol{x}\, \widetilde{\mathcal{P}}_k$	$\mathcal{P}_k$
$(k \ge 0)$	$\boldsymbol{\mathcal{P}}_k \oplus_{i=1}^{ne} \mathbf{curl}\, \Psi_i$	$\mathcal{P}_k$
$(k \ge 1)$	$\boldsymbol{\mathcal{P}}_k \oplus_{i=1}^{ne} \mathbf{curl}\, \Psi_i$	$\mathcal{P}_{k-1}$

As we pointed out in the Introduction, the space $\delta \boldsymbol{V}_{\text{fillM}}$ in Theorem 2.5, defined on a general polygonal element K, depends on a particular edge numbering (and the choice of lifting functions). So, we do get a different space with a different edge numbering and/or a different choice of lifting functions. The dependence on edge numbering is a direct consequence of our edge-by-edge construction of $\delta \boldsymbol{V}_{\text{fillM}}$ as shown in Section 3 which is the only one applicable to an arbitrary polygonal element, Moreover, the superconvergence properties of the associated methods are not compromised at all. However, if the polygon K is a regular convex polygon (isogonal and isotoxal), we might be more interested in finding a space $\delta \boldsymbol{V}_{\text{fillM}}$ which *does not* depend on the edge numbering. We do not concern ourselves with this problem open since it requires case-by-case study of the regular polygon K. However, we our edge-by-edge construction in Section 3 can be used as a starting point to achieve this goal.

Note that even for an element K with hanging nodes, or more generally, when its two edges lie the same line, we can still use the space provided in Theorem 2.5 to define HDG methods even though the spaces do not admit M-decompositions. We expect the superconvergence properties of the resulting method not to be affected for the same reasons that a similar result holds for superconvergent HDG methods on triangular mesh with hanging nodes [11, 12].

When K is a triangle, this construction provides the same spaces than that obtained in Theorem 2.2; when K is a square, it provide the same spaces (with a polynomial lifting function) than those obtained in Theorem 2.3.

Before ending this section, let us compare our space $\boldsymbol{V}^{\text{mix}} \times W^{\text{mix}}$ in the case when K is a convex quadrilateral with the space proposed in [2], which defines the first (rigorously proven) high-order mixed methods on a convex quadrilateral mesh. Such a space is first defined on a unit square $\widehat{K}$ with

$$\boldsymbol{V}(\widehat{K}) := \mathcal{P}_{k+2,k}(\widehat{K}) \times \mathcal{P}_{k,k+2}(\widehat{K}), \quad W(\widehat{K}) := \widehat{\nabla} \cdot \boldsymbol{V}(\widehat{K}),$$

and then constructed on a general convex quadrilateral K using pullback of the bilinear mapping from the reference element $\widehat{K}$ to the physical element K. The resulting space has the property that it contains $\boldsymbol{\mathcal{P}}_k(K) \times \mathcal{P}_k(K)$. Our space does have this property without the need of the pullback mapping as we work directly on the physical element K. The resulting mixed method shares the same convergence rates as that in [2]. However, our space has significantly smaller dimension than that in [2] since

$$\dim \mathcal{P}_{k+2,k}(\widehat{K}) \times \mathcal{P}_{k,k+2}(\widehat{K}) - \dim \boldsymbol{V}^{\text{mix}} = \begin{cases} 2 & \text{if } k = 0, \\ k^2 + 4k + 1 & \text{if } k \geq 1, \end{cases}$$

$$\dim \widehat{\nabla} \cdot \boldsymbol{V}(\widehat{K}) - \dim W^{\text{mix}} = \frac{1}{2}(k^2 + 5k + 4).$$

3. Proofs of Theorems 2.4 and 2.5

In this section, we first prove the negative result of Theorem 2.4, then prove the main result of Theorem 2.5 by carrying out a systematic construction of the spaces $\delta \boldsymbol{V}_{\text{fillM}}$ for $M = \mathcal{P}_k(\partial K)$.

3.1. Proof of Theorem 2.4

We prove Theorem 2.4 by contradiction. Suppose that $\boldsymbol{V}$ is a space of polynomials, $\mathcal{P}_0 \subset W$, and $\boldsymbol{V} \times W$ admits an M-decompositon with $M = \mathcal{P}_k(\partial K)$. By the kernels' trace decomposition in ([20], Thm. 2.8), we have

$$\mathcal{P}_k(\partial K) = \{\boldsymbol{v} \cdot \boldsymbol{n}|_{\partial K} : \boldsymbol{v} \in \boldsymbol{V}, \nabla \cdot \boldsymbol{v} = 0\} \oplus \{w|_{\partial K} : w \in W, \nabla w = \boldsymbol{0}\},$$

where the direct sum is $L^2(\partial K)$-orthogonal. We have $\{w|_{\partial K} : w \in W, \nabla w = \boldsymbol{0}\} = \gamma(\mathcal{P}_0(K))$. So for any $\mu \in \mathcal{P}_0(\partial K) \subset M(\partial K)$ that is a non-zero constant on two edges of K and zero on the other edges, and satisfies $\langle \mu, 1\rangle_{\partial K} = \int_{\partial K} \mu \, \mathrm{ds} = 0$, there exists a divergence-free function in $\boldsymbol{V}$ with normal trace μ. Now, if the element K has two edges that lie on the same line, we can take such $\mu \in \mathcal{P}_0(\partial K)$ to be non-zero on these two edges (with opposite sign) and $\langle \mu, 1\rangle_{\partial K} = 0$. But there is no vector polynomial function such that its normal trace on a line is piecewise constant. This implies that K does not have two edges lie on the same line. Since, in addition, K is not a triangle nor a parallelogram, there exists three edges of K such that their extensions form a triangle. We denote such edges $\mathbf{e}_a, \mathbf{e}_b$, and $\mathbf{e}_c$, with their extended triangle to be T. Let $\mathbf{e}_d$ to be another edge of K.

We take $\mu \in \mathcal{P}_0(\partial K)$ to be non-zero on $\mathbf{e}_a$ and $\mathbf{e}_d$, zero else where, and $\langle \mu, 1\rangle_{\partial K} = 0$, suppose that $\boldsymbol{v} \in \boldsymbol{V}(K)$ is a divergence-free polynomial function such that $\boldsymbol{v}\cdot\boldsymbol{n}|_{\partial K} = \mu$. We have the restriction of the polynomial $\boldsymbol{v}$ (defined on the whole space $\mathbb{R}^2$) on the extended triangle T is still a divergence-free polynomial whose trace is a non-zero constant on (the extension of) edge $\mathbf{e}_a$, and zero on (the extension of) edges $\mathbf{e}_b$ and $\mathbf{e}_c$. But $0 = \int_T \nabla\cdot\boldsymbol{v}\,\mathrm{dx} = \int_{\partial T} \boldsymbol{v}\cdot\boldsymbol{n}\,\mathrm{ds} \neq 0$. This leads to a contradiction. This completes the proof of Theorem 2.4. $\square$

3.2. Proof of Theorem 2.5

We omit the proofs related to the S-index and the space $\delta\boldsymbol{V}_{\mathrm{fillW}}$ for their simplicity, and focus on the proofs for the M-index and the space $\delta\boldsymbol{V}_{\mathrm{fillM}}$.

Here, we begin by developing an algorithm that, given a counter-clockwise ordering of the ne edges of K, $\{\mathbf{e}_i\}_{i=1}^{ne}$, and an initial space $\boldsymbol{V}_g\times W_g$ satisfying the inclusion properties (I) with $\mathcal{P}_0(K)\subset W_g$, provides a space $\delta\boldsymbol{V}_{\mathrm{fillM}}$ satisfying the properties in Table 2. We then apply it to prove the results.

3.2.1. An algorithm to construct the space $\delta\boldsymbol{V}_{\mathrm{fillM}}$

We use the notation introduced in the previous section. For $i = 1,\dots,ne+1$, we define $\boldsymbol{V}_{g_{s,i}}$ to be the divergence-free subspace of $\boldsymbol{V}_g$ with vanishing normal traces on the first $i-1$ edges. In other words,

$$\boldsymbol{V}_{g_{s,i}} := \{\boldsymbol{v}\in\boldsymbol{V}_g:\ \nabla\cdot\boldsymbol{v}=0,\ \boldsymbol{v}\cdot\boldsymbol{n}|_{\mathbf{e}_j}=0,\ 1\le j\le i-1\},\ \text{for } 1\le i\le ne+1.$$

The gradient-free subspace of W_g, $W_{g_{cst}} := \{w\in W_g:\ \nabla w=\mathbf{0}\}$, also plays an important role in the theory of M-decompositions; see the kernels' trace decomposition in ([20], Thm. 2.8). By the inclusion property $\mathcal{P}_0(K)\subset W_g$, we have that $W_{g_{cst}} = \mathcal{P}_0(K)$ is just the space of constants on K. Nevertheless, we prefer to use the special name since in other settings such space might be different.

For $i=1,\dots,ne$, we define $\gamma_i(\boldsymbol{V}) := \{\boldsymbol{v}\cdot\boldsymbol{n}|_{\mathbf{e}_i}:\ \boldsymbol{v}\in\boldsymbol{V}\}$ to be the normal trace of $\boldsymbol{V}$ on $\mathbf{e}_i$, and $\gamma_i(W) := \{w|_{\mathbf{e}_i}:\ w\in W\}$ to be the trace of W on $\mathbf{e}_i$. Note that $\gamma_i(W_{g_{cst}}) = \mathcal{P}_0(\mathbf{e}_i)$ is the space of constants on $\mathbf{e}_i$.

Now, we define the M-index for each edge.

Definition 3.1 (The M-index for each edge)**.** The M-index of the space $\boldsymbol{V}_g\times W_g$ for the ith edge $\mathbf{e}_i$ is the number

$$I_{M,i}(\boldsymbol{V}_g\times W_g) := \dim M(\mathbf{e}_i) - \dim\gamma_i(\boldsymbol{V}_{g_{s,i}}) - \delta_{i,ne}\dim\gamma_{ne}(W_{g_{cst}}),$$

where $\delta_{i,ne}$ is the Kronecker delta.

Since $\boldsymbol{V}_g\times W_g$ satisfies the inclusion properties (I), we have

$$\begin{aligned} \gamma_i(\boldsymbol{V}_{g_{s,i}}) &\subset M(\mathbf{e}_i) \qquad \text{for all } 1\le i\le ne-1,\\ \gamma_{ne}(\boldsymbol{V}_{g_{s,ne}}) + \gamma_{ne}(W_{g_{cst}}) &\subset M(\mathbf{e}_{ne}). \end{aligned}$$

Actually, the sum in the last inclusion is an ($L^2(\mathbf{e}_{ne})$-orthogonal) direct sum: given any $(\boldsymbol{v},w)\in\boldsymbol{V}_{g_{s,ne}}\times W_{g_{cst}}$, we have

$$\langle\gamma_{ne}\boldsymbol{v},\gamma_{ne}w\rangle_{\mathbf{e}_{ne}} = \langle\boldsymbol{v}\cdot\boldsymbol{n},w\rangle_{\mathbf{e}_{ne}} = \langle\boldsymbol{v}\cdot\boldsymbol{n},w\rangle_{\partial K} = (\boldsymbol{v},\nabla w)_K + (\nabla\cdot\boldsymbol{v},w)_K = 0.$$

Using these facts, we immediately get that $I_{M,i}(\boldsymbol{V}_g\times W_g)$ is a natural number for any $1\le i\le ne$.

We are now ready to state our result.

Theorem 3.2. *Set $\delta\boldsymbol{V}_{\mathrm{fillM}} := \oplus_{i=1}^{ne}\delta\boldsymbol{V}^i_{\mathrm{fillM}}$ where*

(α) $\gamma(\delta\boldsymbol{V}^i_{\mathrm{fillM}})\subset M$,
(β) $\nabla\cdot\delta\boldsymbol{V}^i_{\mathrm{fillM}} = \{\mathbf{0}\}$,
(γ.1) $\gamma_j(\delta\boldsymbol{V}^i_{\mathrm{fillM}}) = \{0\}$, *for* $1\le j\le i-1$,
(γ.2) $\gamma_i(\boldsymbol{V}_{g_{s,i}})\cap\gamma_i(\delta\boldsymbol{V}^i_{\mathrm{fillM}}) = \{0\}$,
(δ) $\dim\delta\boldsymbol{V}^i_{\mathrm{fillM}} = \dim\gamma_i(\delta\boldsymbol{V}^i_{\mathrm{fillM}}) = I_{M,i}(\boldsymbol{V}_g\times W_g)$.

Then $\delta \boldsymbol{V}_{\text{fillM}}$ satisfies the properties in Table 2, that is,

(a) $\gamma\delta \boldsymbol{V}_{\text{fillM}} \subset M$,
(b) $\nabla\cdot\delta \boldsymbol{V}_{\text{fillM}} = \{0\}$,
(c) $\gamma \boldsymbol{V}_{g_{s,1}} \cap \gamma\delta \boldsymbol{V}_{\text{fillM}} = \{0\}$,
(d) $\dim\delta \boldsymbol{V}_{\text{fillM}} = \dim\gamma\delta \boldsymbol{V}_{\text{fillM}} = I_M(\boldsymbol{V}_g \times W_g)$.

This result implies that $\boldsymbol{V}_g \oplus \delta\boldsymbol{V}_{\text{fillM}} \times W_g$ admits an M-decompositon, see ([20], Prop. 5.1).

Proof. Properties (a), (b) and (c) follow directly form properties (α), (β) and (γ), respectively. It remains to prove property (d). But, we have

$$\dim\delta \boldsymbol{V}_{\text{fillM}} = \sum_{i=1}^{ne} \dim\delta \boldsymbol{V}^i_{\text{fillM}} = \sum_{i=1}^{ne} I_{M,i}(\boldsymbol{V}_g\times W_g) = \sum_{i=1}^{ne} \dim\gamma_i\delta \boldsymbol{V}^i_{\text{fillM}} = \dim\gamma\delta \boldsymbol{V}_{\text{fillM}},$$

and, by the definition of $I_{M,i}(\boldsymbol{V}_g \times W_g)$, we get

$$\begin{aligned}
\dim\delta \boldsymbol{V}_{\text{fillM}} =\ & \dim M - \sum_{i=1}^{ne} \dim\gamma_i(\boldsymbol{V}_{g_{s,i}}) - \dim\gamma_{ne}(W_{g_{cst}}) \\
=\ & \dim M - \sum_{i=1}^{ne}(\dim \boldsymbol{V}_{g_{s,i}} - \dim \boldsymbol{V}_{g_{s,i+1}}) - \dim\gamma_{ne}(W_{g_{cst}}) \\
=\ & \dim M - (\dim \boldsymbol{V}_{g_{s,1}} - \dim \boldsymbol{V}_{g_{s,ne+1}}) - \dim\gamma_{ne}(W_{g_{cst}}).
\end{aligned}$$

Finally, by the definition of the spaces $\boldsymbol{V}_{g_{s,1}}$ and $\boldsymbol{V}_{g_{s,ne+1}}$, we get

$$\begin{aligned}
\dim\delta \boldsymbol{V}_{\text{fillM}} =\ & \dim M - (\dim\{\boldsymbol{v}\in \boldsymbol{V}_g :\ \nabla\cdot\boldsymbol{v} = 0\} \\
& - \dim\{\boldsymbol{v}\in \boldsymbol{V}_g :\ \nabla\cdot\boldsymbol{v} = 0, \boldsymbol{v}\cdot\boldsymbol{n}|_{\partial K} = 0\}) - \dim\gamma_{ne}(W_{g_{cst}}). \\
=\ & \dim M - \dim\{\boldsymbol{v}\cdot\boldsymbol{n}|_{\partial K} : \boldsymbol{v}\in \boldsymbol{V}_g,\ \nabla\cdot\boldsymbol{v} = 0\} \\
& - \dim\{w|_{\partial K} : w\in W_g, \nabla w = \boldsymbol{0}\} \\
=\ & I_M(\boldsymbol{V}_g\times W_g).
\end{aligned}$$

This completes the proof. $\square$

Based on this result, we have that the following algorithm provides a practical construction of the filling space $\delta \boldsymbol{V}_{\text{fillM}}$.

3.2.2. Application of Algorithm PC

Now, we apply Algorithm PC to the setting in Theorem 2.5, that is, K is a star-shaped polygon K of ne edges without edges lie on the same line, $M = \mathcal{P}_k(\partial K)$ and $\boldsymbol{V}_g \times W_g = \boldsymbol{\mathcal{P}}_k \times \mathcal{P}_k$. We proceed to find the space $\delta \boldsymbol{V}_{\text{fillM}}$ in three steps.

1. Finding the spaces $\boldsymbol{V}_{g_{\mathsf{s,i}}}$. The spaces $\boldsymbol{V}_{g_{\mathsf{s,i}}}$ are characterized in the following result.

Proposition 3.3. *We have that*

$$\boldsymbol{V}_{g_{s,i}} = \mathbf{curl}\,\Phi_i,$$

where $\Phi_i := \{b_{i-1}\phi_i :\ \phi_i \in \mathcal{P}_{k+2-i}(K)\}$. Here $b_0 = 1$, and $b_i := \Pi_{j=1}^{i}\lambda_j$.

Algorithm PC. A practical construction of $\delta \boldsymbol{V}_{\text{fillM}}$.

Input: A counter-clockwise ordering of the ne edges of the polygon K, $\{\mathbf{e}_i\}_{i=1}^{ne}$.
Input: The space of traces M.
Input: A space $\boldsymbol{V}_g \times W_g$ satisfying the inclusion properties (I).
Output: The space $\delta \boldsymbol{V}_{\text{fillM}}$.

For each $i = 1, \dots, ne$,
(1) Find the auxiliary spaces $\boldsymbol{V}_{g_{s,i}}$.
(2) Find an $I_{M,i}(\boldsymbol{V}_g \times W_g)$-dimensional complement space $C_{M,i}$ on edge $\mathbf{e}_i$:

$$\gamma_i(\boldsymbol{V}_{g_{s,i}}) \oplus C_{M,i} = \widetilde{M}(\mathbf{e}_i),$$

here $\widetilde{M}(\mathbf{e}_i) = M(\mathbf{e}_i)$ if $i < ne$, and $\widetilde{M}(\mathbf{e}_{ne}) = \gamma_{ne}(W_{g_{cst}})^{\perp}$ is the subspace of $M(\mathbf{e}_{ne})$ that is $L^2(\mathbf{e}_{ne})$-orthogonal to $\gamma_{ne}(W_{g_{cst}}) = \mathcal{P}_0(\mathbf{e}_{ne})$.
(3) Find an $I_{M,i}(\boldsymbol{V}_g \times W_g)$-dimensional, divergence-free filling space $\delta \boldsymbol{V}^i_{\text{fillM}}$ on K:

$$\begin{aligned} &(3.1)\ \ \gamma_j(\delta \boldsymbol{V}^i_{\text{fillM}}) = \{0\}, \qquad \text{for } 1 \le j \le i-1,\\ &(3.2)\ \ \gamma_i(\delta \boldsymbol{V}^i_{\text{fillM}}) = C_{M,i},\\ &(3.3)\ \ \gamma_j(\delta \boldsymbol{V}^i_{\text{fillM}}) \subset M(\mathbf{e}_j), \ \ \text{for } i+1 \le j \le ne. \end{aligned}$$

(The space $\delta \boldsymbol{V}^i_{\text{fillM}}$ satisfies properties (α)–(δ) of Thm. 3.2.)
return $\delta \boldsymbol{V}_{\text{fillM}} := \oplus_{i=1}^{ne} \delta \boldsymbol{V}^i_{\text{fillM}}$.

Proof. Since $\boldsymbol{V}_g = \boldsymbol{\mathcal{P}}_k$, it is easy to show

$$\mathbf{curl}\, \Phi_i \subset \boldsymbol{V}_{g_{s,i}} \subset \mathbf{curl}\, \mathcal{P}_{k+1}.$$

Since $\Phi_1 = \mathcal{P}_{k+1}$, the reverse inclusion, $\boldsymbol{V}_{g_{s,i}} \subset \mathbf{curl}\, \Phi_i$, is true for $i = 1$.

Now, let us prove the reverse inclusions for $i \ge 2$. We use the following simple fact:

$$\gamma_i(\mathbf{curl}\, \phi) = 0 \quad \Longleftrightarrow \quad \gamma_i\, \phi \in \mathcal{P}_0(\mathbf{e}_i) \qquad \text{for any } \phi \in H^1(K) \text{ and any edge } \mathbf{e}_i \text{ of } K.$$

Let $\boldsymbol{v} = \mathbf{curl}\, \phi \in \boldsymbol{V}_{g_{s,i}}$ with $\phi \in \mathcal{P}_{k+1}$. We have $\gamma_j(\mathbf{curl}\, \phi) = 0$ for $1 \le j \le i-1$. Hence, $\gamma_j\ \phi \in \mathcal{P}_0(\mathbf{e}_j)$ for $1 \le j \le i-1$. Since ϕ is defined up to a constant, we can assume $\phi(\mathbf{v}_1) = 0$. This immediately implies $\gamma_j\ \phi = 0$ for $1 \le j \le i-1$, hence $\phi = b_{i-1}\widetilde{\phi}$ for some $\widetilde{\phi} \in \mathcal{P}_{k+2-i}(K)$. This completes the proof. $\square$

2. Finding the complement spaces $\boldsymbol{C_{M,i}}$. We know that the space $C_{M,i}$ is any subspace of $\widetilde{M}(\mathbf{e}_i)$ such that $\gamma_i(\boldsymbol{V}_{g_{s,i}}) \oplus C_{M,i} = \widetilde{M}(\mathbf{e}_i)$; see the definition of $\widetilde{M}(\mathbf{e}_i)$ in Algorithm PC. Since $M(\mathbf{e}_i) = \mathcal{P}_k(\mathbf{e}_i)$, we need first to characterize $\gamma_i(\boldsymbol{V}_{g_{s,i}})$ then to find a choice of $C_{M,i}$, which is not necessarily unique. The characterization of $\gamma_i(\boldsymbol{V}_{g_{s,i}})$ is contained in the following corollary of the previous proposition.

Corollary 3.4. *We have, for* $1 \le i \le ne$,

$$\begin{aligned} \gamma_i(\boldsymbol{V}_{g_{s,i}}) &= \operatorname{span}\{\gamma_i(\mathbf{curl}\, b_{i-1}\lambda^a_{i+1})\}_{a=\delta_{1,i}}^{k+2-i},\\ \dim \gamma_i(\boldsymbol{V}_{g_{s,i}}) &= \dim \mathcal{P}_{k+2-i}(\mathbf{e}_i) - \delta_{1,i},\\ I_{M,i}(\boldsymbol{V}_g \times W_g) &= \min{(k+1, i-2)} + \delta_{1,i} - \delta_{ne,i}. \end{aligned}$$

Here, we use the convention that $\dim \mathcal{P}_m = 0$ for any negative integer m.

Proof. The first identity follows from the definition of the auxiliary space $\boldsymbol{V}_{g_{s,i}}$, and the third follows from the second identity and the definition of the M-index on edge $\mathbf{e}_i$, $I_{M,i}(\boldsymbol{V}_g \times W_g)$. Let us prove the second. By construction,

$$\begin{aligned}\dim \gamma_i(\boldsymbol{V}_{g_{s,i}}) &= \dim \boldsymbol{V}_{g_{s,i}} - \dim \boldsymbol{V}_{g_{s,i+1}}\\ &= \dim \boldsymbol{V}_{g_{s,i}} - \dim \boldsymbol{V}_{g_{s,i+1}}\\ &= (\dim \mathcal{P}_{k+2-i}(K) - \delta_{1,i}) - (\dim \mathcal{P}_{k+1-i}(K) - \delta_{1,i+1})\\ &= \dim \mathcal{P}_{k+2-i}(\mathbf{e}_i) - \delta_{1,i},\end{aligned}$$

since $\dim \boldsymbol{V}_{g_{s,i}} = \dim \mathcal{P}_{k+2-i}(K) - \delta_{1,i}$. This completes the proof. □

Now, we give a particular choice of the trace space $C_{M,i}$ in the following result.

Theorem 3.5. *The following $I_{M,i}(\boldsymbol{V}_g \times W_g)$-dimensional spaces $C_{M,i}$ of functions defined on the edge $\mathbf{e}_i$ satisfy $\gamma_i(\boldsymbol{V}_{g_{s,i}}) \oplus C_{M,i} = \widetilde{M}(\mathbf{e}_i)$ where*

$$C_{M,i} = \begin{cases} \{0\} & \text{if } i \le 2,\\ \operatorname{span}\{\gamma_i(\mathbf{curl}\,\lambda_{i-1}\lambda_{i+1}^b) : \max\{k+3-i, 0\} + \delta_{ne,i} \le b \le k\} & \text{if } i \ge 3.\end{cases}$$

Proof. It is easy to check that $\dim C_{M,i} = I_{M,i}(\boldsymbol{V}_g \times W_g)$ and $C_{M,i} \subset \widetilde{M}(\mathbf{e}_i)$. We are left to show that $\gamma_i(\boldsymbol{V}_{g_{s,i}}) \cap C_{M,i} = \{0\}$. We prove this result for the case that $3 \le i \le ne-1$ and $k \ge i-3$. The other cases are similar and simpler.

To show $\gamma_i(\boldsymbol{V}_{g_{s,i}}) \cap C_{M,i} = \{0\}$, we only need to prove the linear independence of the following two sets

$$\{\gamma_i(\mathbf{curl}\, b_{i-1}\lambda_{i+1}^a)\}_{a=0}^{k+2-i} \text{ and } \{\gamma_i(\mathbf{curl}\,\lambda_{i-1}\lambda_{i+1}^b)\}_{b=k+3-i}^{k},$$

here the left is a set of bases for $\gamma_i(\boldsymbol{V}_{g_{s,i}})$ and the right is a set of bases for $C_{M,i}$. Let us assume that there exist constants $\{C_a\}_{a=0}^{k+2-i}$ and $\{D_b\}_{b=k+3-i}^{k}$ such that

$$\gamma_i\left(\sum_{a=0}^{k+2-i} C_a\,\mathbf{curl}\, b_{i-1}\lambda_{i+1}^a + \sum_{b=k+3-i}^{k} D_b\,\mathbf{curl}\,\lambda_{i-1}\lambda_{i+1}^b\right) = 0.$$

That is,

$$\left(\sum_{a=0}^{k+2-i} C_a\, b_{i-1}\lambda_{i+1}^a + \sum_{b=k+3-i}^{k} D_b\,\lambda_{i-1}\lambda_{i+1}^b\right)\Big|_{\mathbf{e}_i} \in \mathcal{P}_0(\mathbf{e}_i).$$

Hence,

$$\lambda_{i-1}\left(\sum_{a=0}^{k+2-i} C_a\, b_{i-2}\lambda_{i+1}^a + \sum_{b=k+3-i}^{k} D_b\,\lambda_{i+1}^b\right)\Big|_{\mathbf{e}_i} \in \mathcal{P}_0(\mathbf{e}_i).$$

This implies

$$\left(\sum_{a=0}^{k+2-i} C_a\, b_{i-2}\lambda_{i+1}^a + \sum_{b=k+3-i}^{k} D_b\,\lambda_{i+1}^b\right)\Big|_{\mathbf{e}_i} = 0.$$

Now, evaluating the expression at the node $\mathbf{v}_{i+1} = \mathbf{e}_i \cap \mathbf{e}_{i+1}$, we get $C_0 = 0$ since $b_{i-2}(\mathbf{v}_{i+1}) \neq 0$ and $\lambda_{i+1}(\mathbf{v}_{i+1}) = 0$. Then, dividing the expression by λ_{i+1} and evaluating the resulting expression again at $\mathbf{v}_{i+1} = \mathbf{e}_i \cap \mathbf{e}_{i+1}$, we get $C_1 = 0$. Similarly, we get $C_a = 0$ for $a = 2, \ldots, k+2-i$, and $D_b = 0$ for $b = k+3-i, \ldots, k$. This completes the proof. □

3. Finding the filling spaces $\delta\boldsymbol{V}^i_{\mathbf{fillM}}$. Now, it is easy to show that the divergence-free space $\delta\boldsymbol{V}^i_{\mathrm{fillM}} := \mathbf{curl}\,\Psi_i$ satisfies the trace properties (3.1-3.3) in Algorithm PC and has dimension $I_{M,i}(\boldsymbol{V}_g \times W_g)$, where Ψ_i is defined in Theorem 2.5. Indeed, using conditions (L) of ξ_{i+1}, the equality (3.1) is true since $\gamma_j(\xi_{i+1}) = 0$ for $j \le i-1$, the equality (3.2) is true since $\gamma_i(\xi_{i+1}) = \frac{\gamma_i(\lambda_{i-1})}{\lambda_{i-1}(\mathbf{v}_{i+1})}$, and the equality (3.3) is true since $\gamma_j(\xi_{i+1}) \in \mathcal{P}_1(\mathbf{e}_j)$ for $j \ge i+1$. Hence, $\delta\boldsymbol{V}_{\mathrm{fillM}}$ of Theorem 2.5 satisfies properties in Table 2.

The computation of the dimension of $\delta\boldsymbol{V}_{\mathbf{fillM}}$. We end this subsection by computing the dimension of $\delta\boldsymbol{V}_{\mathrm{fillM}}$. We have

$$\begin{aligned}
\dim\delta\boldsymbol{V}_{\mathrm{fillM}} &= \sum_{i=1}^{ne} \dim\delta\boldsymbol{V}^i_{\mathrm{fillM}} \\
&= \sum_{i=1}^{ne} I_{M,i}(\boldsymbol{V}_g \times W_g) = \sum_{i=1}^{ne} (\min\{k+1, i-2\} + \delta_{1,i} - \delta_{ne,i}) \\
&= \sum_{i=3}^{ne} (\min\{k, i-3\} + 1 - \delta_{ne,i}) = \sum_{j=0}^{ne-3} (\min\{k,j\}+1) - 1 \\
&= \sum_{j=1}^{ne-3} \min\{k,j\} + (ne-3).
\end{aligned}$$

If we set $\theta := \min\{k, ne-3\}$, we can write

$$\begin{aligned}
\dim\delta\boldsymbol{V}_{\mathrm{fillM}} &= \sum_{j=1}^{\theta} \min\{k,j\} + \sum_{j=\theta+1}^{ne-3} \min\{k,j\} + (ne-3) \\
&= \sum_{j=1}^{\theta} j + \sum_{j=\theta+1}^{ne-3} \theta + (ne-3) \\
&= \frac{1}{2}\theta(\theta+1) + \theta\,(ne-3-\theta) + (ne-3) \\
&= (\theta+1)\,(ne-3) - \frac{1}{2}\theta(\theta-1).
\end{aligned}$$

This completes the proof of Theorem 2.5. □

4. Extensions

In this section, we present some extensions of our constructions in Section 2. First, we take a closer look at the case with quadrilateral elements. Then, we consider the case of the space M for which the polynomials have different degrees in different edges.

4.1. Convex quadrilaterals without hanging nodes

For $k \ge 1$, Theorem 2.5 gives the following two-dimensional filling space:

$$\delta\boldsymbol{V}_{\mathrm{fillM}} = \mathbf{curl}\,\mathrm{span}\{\xi_4\lambda_4^k, \xi_1\lambda_1^k\}.$$

In order to be able to use only one lifting function and save computational effort, we can slightly modify this space to be

$$\delta\boldsymbol{V}_{\mathrm{fillM}} = \mathbf{curl}\,\mathrm{span}\{\xi_4\lambda_4^k, \xi_4\lambda_3^k\}.$$

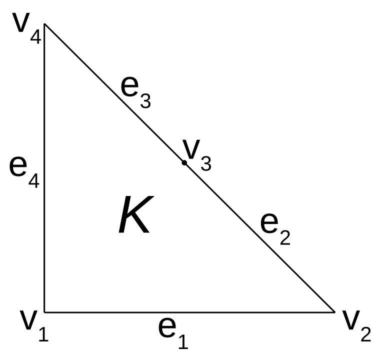

FIGURE 2. A quadrilateral collapsed into a triangle with a hanging node.

Thus, instead of using two lifting functions ξ_4 and ξ_1, we only use one, ξ_4. Moreover, we can subdivde the quadrilateral into two triangles and define the composite lifting function ξ_4 based on this subdivision to save computational cost in numerical integration.

4.2. Triangles with one hanging node

When a quadrilateral collapses into a triangle with a hanging node, see Figure 2, the results in Corollary 3.4 do not apply anymore, and the spaces provided in Theorem 2.5 do not admit M-decompositions. Let us obtain an M-decomposition for this case with $\boldsymbol{V}_g \times W_g = \boldsymbol{\mathcal{P}}_k \times \mathcal{P}_k$ and $M = \mathcal{P}_k(\partial K)$.

To do that, let the element nodes ordered as in Fig 2. Using Proposition 3.3, we can easily get that $I_{M,i} = 0$ for $i = 1, 2, 4$, that$I_{M,3} = k + 1$, and that the $(k + 1)$-dimensional filling space can be taken as

$$\delta \boldsymbol{V}_{\text{fillM}} = \textbf{curl}\,\text{span}\{\xi_4 \lambda_4^b; 0 \le b \le k\}.$$

Here ξ_4 can be chosen as a composite lifting.

Note that instead of two (one for the $k = 0$ case) additional basis functions, we have $k+1$. When $k = 0$, this filling space has dimension one and is the same as the one provided by Theorem 2.5. When $k = 1$, this filling space has the same dimension as the one in Theorem 2.5, namely, two, but has different basis functions.

4.3. Variable-degree trace space $M(\partial K)$

Now, we consider the local space

$$M(\partial K) := \{\mu \in L^2(\partial K) : \mu|_{\mathbf{e}} \in \mathcal{P}_{k_{\mathbf{e}}}(\mathbf{e}),\ \text{for all edges } \mathbf{e} \text{ of } K\},$$

where $k_{\mathbf{e}} \ge 0$ can vary from edge to edge. Note that this choice of $M(\partial K)$ comes naturally in the context of p-adaptivity.

Next we show that the construction of an M-decomposition is just a *simple* modification of that of the uniform degree case. For the sake of simplicity, let us take K to be a triangle; the construction for a general polygon is similar. We take as initial guess the space $\boldsymbol{V}_g \times W_g = \boldsymbol{\mathcal{P}}_k(K) \times \mathcal{P}_k(K)$ where $k := \min\{k_e :$ for all edges $\boldsymbol{e}$ of K$\}$. This space admits an M-decomposition with $M(\partial K) = \mathcal{P}_k(\partial K)$. Then, the M-indexes for the variable trace space for each edge are $I_{M,i} = k_{\mathbf{e}_i} - k$ for $i = 1, 2, 3$. Since the complement spaces $C_{M,i}$ can be chosen as

$$C_{M,i} = \text{span}\,\{\gamma_i(\lambda_{i-1}\lambda_{i+1}^b) :\ k + 1 \le b \le k_{\mathbf{e}_i}\},$$

the filling space can be taken as

$$\delta \boldsymbol{V}_{\text{fillM}} := \oplus_{i=1}^3 \,\textbf{curl}\,\text{span}\{\lambda_{i-1}\lambda_{i+1}^b; k + 1 \le b \le k_{\mathbf{e}_i}\}.$$

Note that its dimension is $\sum_{i=1}^3 (k_{\mathbf{e}_i} - k)$.

5. Numerical results

In this section, we present numerical results for the model problem

$$\begin{aligned} -\Delta u &= f \quad \text{in } \Omega, \\ u &= g \quad \text{on } \partial\Omega, \end{aligned}$$

where Ω is a unit square, and the exact solution is $u(x,y) = \sin(2\pi x)\sin(2\pi y)$.

We present numerical results for four HDG methods along with two hybridized mixed methods fitting the formulation (1.1) whose corresponding spaces and stabilization operator, and the expected convergence rates are listed in Table 8. The first method is denoted by LDG-H [17]. We denote the second method as LS since it is originally from Lehrenfeld's diploma thesis [28] (with a primal formulation) under the direction of Schöberl. The third method is denoted as HHO since the key idea stems from the Hybrid-High Order(HHO) methods [22]. Here the linear operator $r_{\partial K}$ is defined as follows: $r_{\partial K}(u_h - \widehat{u}_h) := P_M\left(p_h^{k+1}(u_h, \widehat{u}_h)\right) - \widehat{u}_h$, where $p_h^{k+1}(u_h, \widehat{u}_h) \in \mathcal{P}_{k+1}(K)$ satisfies

$$\begin{aligned} (p_h^{k+1}(u_h, \widehat{u}_h), w)_K &= (u_h, w)_K && \forall w \in \mathcal{P}_k(K), \\ (\nabla p_h^{k+1}(u_h, \widehat{u}_h), \nabla z)_K &= -(u_h, \Delta z)_K + \langle \widehat{u}_h, \nabla z \cdot \boldsymbol{n}\rangle_{\partial K} && \forall z \in \{w \in \mathcal{P}_{k+1}(K) : \ w \perp \mathcal{P}_k(K)\}. \end{aligned}$$

This is a slight variation of the original HHO flux introduced in [22], see also [21], there the method is devised for the primal formulation, but can be identified as a mixed formulation with the approximate flux space $\boldsymbol{V}$ taken to be the gradients $\nabla\mathcal{P}_{k+1}(K)$ and the approximate flux satisfies $\boldsymbol{q}_h = -\nabla p_h^{k+1}(u_h, \widehat{u}_h)$. We denote the fourth method as HDG-M since it is the HDG method that use spaces admitting M-decompositions. Here we use the composite lifting functions for star-shaped polygons in Section 2 to define the lifting functions in $\delta\boldsymbol{V}_{\text{fillM}}$. The fifth and sixth methods are the two (hybridized) mixed methods that *sandwich* HDG-M; we denote them as L-MIX (lower mixed method) and U-MIX (upper mixed method) respectively. We refer to ([20], Thm. 6.3) for a close relation among the last three methods, HDG-M, L-MIX, and U-MIX. Note that on a triangular mesh, HDG-M is nothing but LDG-H since $\delta\boldsymbol{V}_{\text{fillM}} = 0$, L-MIX is nothing but the (hybridized) BDM method [7], and U-MIX is nothing but the (hybridized) RT method [31].

For all the methods, the postprocessing $u_h^* \in \mathcal{P}_{k+1}(K)$ is chosen to be the function that satisfy

$$\begin{aligned} (u_h^*, w)_K &= (u_h, w)_K && \forall w \in \mathcal{P}_0(K), \\ (\nabla u_h^*, \nabla z)_K &= -(\boldsymbol{q}_h, \nabla z)_K && \forall z \in \mathcal{P}_{k+1}(K). \end{aligned}$$

Since the choice of the trace space $M(F)$ is the same for all the methods, their global linear system (for $\widehat{u}_h$) have exactly the same size and sparsity pattern on the same mesh; we observe similar condition numbers

Table 8. The local spaces $\boldsymbol{V}(K) \times W(K)$ and stabilization operator α with $M(\partial K) = \mathcal{P}_k(\partial K)$ for the four HDG methods and their expected convergence rates in $L^2(\Omega)$-error of the approximate flux $\boldsymbol{q}_h$ and postprocessed scalar u_h^*.

	$\boldsymbol{V}$	W	$\alpha(u_h - \widehat{u}_h)$	$\Vert\boldsymbol{q} - \boldsymbol{q}_h\Vert_\Omega$	$\Vert u - u_h^*\Vert_\Omega$
LDG-H[17]	$\boldsymbol{\mathcal{P}}_k$	$\mathcal{P}_k$	$u_h - \widehat{u}_h$	$k + 1/2$	$k+1$
LS[28,30]	$\boldsymbol{\mathcal{P}}_k$	$\mathcal{P}_{k+1}$	$\frac{1}{h}(P_M u_h - \widehat{u}_h)$	$k+1$	$k+2$
HHO[21,22]	$\boldsymbol{\mathcal{P}}_k$	$\mathcal{P}_k$	$r_{\partial K}^* \frac{1}{h} r_{\partial K}(u_h - \widehat{u}_h)$	$k+1$	$k+2$
HDG-M	$\boldsymbol{\mathcal{P}}_k \oplus \delta\boldsymbol{V}_{\text{fillM}}$	$\mathcal{P}_k$	$u_h - \widehat{u}_h$	$k+1$	$k+2$
L-MIX	$\boldsymbol{\mathcal{P}}_k \oplus \delta\boldsymbol{V}_{\text{fillM}}$	$\mathcal{P}_{k-1}$	0	$k+1$	$\begin{cases} k+1 & \text{if } k=1 \\ k+2 & \text{if } k \geq 2 \end{cases}$
U-MIX	$\boldsymbol{\mathcal{P}}_k \oplus \delta\boldsymbol{V}_{\text{fillM}} \oplus \delta\boldsymbol{V}_{\text{fillW}}$	$\mathcal{P}_k$	0	$k+1$	$k+2$

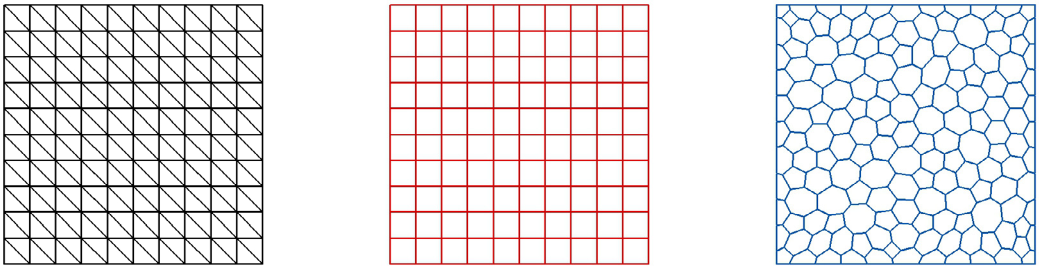

FIGURE 3. Three types of initial meshes. *Left*: a triangular mesh. *Middle*: a square mesh. *Right*: a polygonal mesh.

for all the methods. Hence, solving the global linear system for all the methods, which is the bottleneck of the computation, is expected to take similar time.

While all of these six methods are well-defined on a polygonal meshes, the LDG-H method can be shown to provide suboptimal convergence rate of $k + 1/2$ for the L^2-error in the flux variable $\boldsymbol{q}_h$, and suboptimal convergence rate of $k+1$ for the L^2-error in the postprocessed scalar variable u_h^*, while the other five methods provide optimal convergence rate of $k+1$ for $\boldsymbol{q}_h$ and $k+2$ for u_h^* (when $k = 1$, L-MIX only provide suboptimal convergence rate of $k + 1$ for u_h^*). See [10] for an analysis of the LDG-H method, [30] for an analysis of the LS method and [22] HHO (where the space for the flux is replaced by a much smaller space), and [20] for an analysis of the last three methods.

For all the methods, we solve the problem on triangular, square, and polygonal meshes with the coarsest meshes depicted in Figure 3. Here numerical integration on a polygon K is done by first subdiving the polygon into a set of triangles, and sum up the integral on each triangle using standard quadrature rules for polynomials on triangles. Since we use composite lifting functions on the subdivision of the polygon in the definition of $\delta\boldsymbol{V}_{\mathrm{fillM}}$, the restriction on each subtriangle of these functions are polynomials. Hence the functions in $\delta\boldsymbol{V}_{\mathrm{fillM}}$ are easy to implement. If the element K is a triangle or a parallelogram, we use the standard mapping technique to compute the integrals. The history of convergence for the L^2-error in the flux variable $\boldsymbol{q}_h$ and the postprocessed scalar variable u_h^* is given in Table 9 to 11 for these three types of meshes.

Table 9 presents the history of convergence for the six methods on triangular meshes for $k = 1$ and $k = 2$. We observe expected convergence rates. When $k = 1$, we have second-order convergence rate in $\boldsymbol{q}_h$ for all the methods, and third-order convergence rate in u_h^* for all the methods except L-MIX, for which the convergence rate is second order. When $k = 2$, we have third-order convergence rate in $\boldsymbol{q}_h$ and fourth-order convergence rate in u_h^* for all the methods. The errors in $\boldsymbol{q}_h$ for LDG-H(=HDG-M), LS, and HHO are about the same, those for L-MIX are slightly bigger and those for U-MIX slightly smaller. The errors in u_h^* for LDG-H(=HDG-M), LS, HHO, and U-MIX are about the same, and those for L-MIX are significantly bigger (even for $k = 2$) for the same convergence rates.

Table 10 presents the history of convergence for the six methods on square meshes for $k = 1$ and $k = 2$. We observe slightly better convergence rates than predicted by the theory for LDG-H, and expected convergence rates for the other five methods. When $k = 1$, we have about 1.7 convergence rate in $\boldsymbol{q}_h$ for LDG-H and second-order convergence rate for the other five methods, and about 2.7 convergence rate in u_h^* for LDG-H, second-order convergence rate for L-MIX, and third-order convergence for the other four methods. When $k = 2$, we have about 2.7 convergence rate in $\boldsymbol{q}_h$ for LDG-H and third-order convergence rate for the other five methods, and about 3.8 convergence rate in u_h^* for LDG-H and fourth-order convergence for the other five the methods. The method LDG-H produces the biggest errors in $\boldsymbol{q}_h$. For the other five methods, the errors in $\boldsymbol{q}_h$ for HDG-M, LS, and HHO are about the same, those for L-MIX are slightly bigger, and those for U-MIX slightly smaller.

TABLE 9. History of convergence on triangular meshes.

k	Mesh n	$\|\boldsymbol{q}-\boldsymbol{q}_h\|_{\mathcal{T}_h}$ error	order	$\|u-u_h^*\|_{\mathcal{T}_h}$ error	order	$\|\boldsymbol{q}-\boldsymbol{q}_h\|_{\mathcal{T}_h}$ error	order	$\|u-u_h^*\|_{\mathcal{T}_h}$ error	order	$\|\boldsymbol{q}-\boldsymbol{q}_h\|_{\mathcal{T}_h}$ error	order	$\|u-u_h^*\|_{\mathcal{T}_h}$ error	order
		LDG-H				LS				HHO			
1	10	1.26E-1	–	1.53E-3	–	1.17E-1	–	1.26E-3	–	1.16E-1	–	1.30E-3	–
	20	3.18E-2	1.99	1.84E-4	3.06	2.96E-2	1.98	1.58E-4	3.00	2.92E-2	1.99	1.59E-4	3.04
	40	7.95E-3	2.00	2.25E-5	3.03	7.43E-3	2.00	1.97E-5	3.00	7.31E-3	2.00	1.98E-5	3.01
	80	1.99E-3	2.00	2.78E-6	3.02	1.86E-3	2.00	2.46E-6	3.00	1.83E-3	2.00	2.46E-6	3.00
2	10	1.12E-2	–	1.07E-4	–	1.05E-2	–	9.47E-5	–	1.02E-2	–	9.59E-5	–
	20	1.41E-3	2.99	6.65E-5	4.00	1.32E-3	2.98	6.02E-6	3.98	1.29E-3	2.99	6.04E-6	3.99
	40	1.76E-4	3.00	4.15E-7	4.00	1.66E-4	3.00	3.78E-7	3.99	1.61E-4	3.00	3.78E-7	4.00
	80	2.20E-5	3.00	2.59E-8	4.00	2.08E-5	3.00	2.36E-8	4.00	2.02E-5	3.00	2.37E-8	4.00
		HDG-M = LDG-H				L-MIX = BDM				U-MIX = RT			
1	10	1.26E-1	–	1.53E-3	–	2.47E-1	–	2.30E-2	–	7.18E-2	–	1.30E-3	–
	20	3.18E-2	1.99	1.84E-4	3.06	6.32E-2	1.96	5.91E-3	1.96	1.80E-2	2.00	1.60E-4	3.03
	40	7.95E-3	2.00	2.25E-5	3.03	1.59E-2	1.99	1.49E-3	1.99	4.51E-3	2.00	1.98E-5	3.01
	80	1.99E-3	2.00	2.78E-6	3.02	3.98E-3	2.00	3.73E-4	2.00	1.13E-3	2.00	2.47E-6	3.00
2	10	1.12E-2	–	1.07E-4	–	1.53E-2	–	4.26E-4	–	5.01E-3	–	9.59E-5	–
	20	1.41E-3	2.99	6.65E-5	4.00	1.94E-3	2.98	2.74E-5	3.96	6.28E-4	2.99	6.04E-6	3.99
	40	1.76E-4	3.00	4.15E-7	4.00	2.44E-4	2.99	1.73E-6	3.99	7.87E-5	3.00	3.78E-7	4.00
	80	2.20E-5	3.00	2.59E-8	4.00	3.05E-5	3.00	1.08E-7	4.00	9.84E-6	3.00	2.37E-8	4.00

TABLE 10. History of convergence on square meshes.

k	Mesh n	$\|\boldsymbol{q}-\boldsymbol{q}_h\|_{\mathcal{T}_h}$ error	order	$\|u-u_h^*\|_{\mathcal{T}_h}$ error	order	$\|\boldsymbol{q}-\boldsymbol{q}_h\|_{\mathcal{T}_h}$ error	order	$\|u-u_h^*\|_{\mathcal{T}_h}$ error	order	$\|\boldsymbol{q}-\boldsymbol{q}_h\|_{\mathcal{T}_h}$ error	order	$\|u-u_h^*\|_{\mathcal{T}_h}$ error	order
		LDG-H				LS				HHO			
1	10	3.56E-1	–	8.32E-3	–	1.83E-1	–	2.81E-3	–	1.85E-1	–	2.65E-3	–
	20	1.26E-1	1.50	1.63E-3	2.36	4.42E-2	2.05	2.98E-4	3.24	4.42E-2	2.06	2.88E-4	3.21
	40	4.21E-2	1.58	2.83E-4	2.52	1.09E-2	2.02	3.41E-5	3.13	1.09E-3	2.02	3.37E-5	3.09
	80	1.29E-2	1.71	4.41E-5	2.68	2.71E-3	2.01	4.15E-6	3.04	2.71E-3	2.01	4.13E-6	3.03
2	10	3.62E-2	–	2.63E-4	–	1.84E-2	–	1.86E-4	–	1.86E-2	–	1.88E-4	–
	20	6.42E-3	2.50	2.02E-5	3.71	2.23E-3	3.04	1.16E-5	4.00	2.23E-3	3.05	1.17E-5	4.01
	40	1.06E-3	2.60	1.53E-6	3.72	2.75E-4	3.02	7.25E-7	4.00	2.75E-4	3.02	7.26E-7	4.01
	80	1.60E-4	2.73	1.11E-7	3.79	3.42E-5	3.01	4.53E-8	4.00	3.42E-5	3.01	4.53E-8	4.00
		HDG-M				L-MIX				U-MIX			
1	10	1.75E-1	–	2.59E-3	–	3.67E-1	–	3.09E-2	–	7.52E-2	–	2.19E-3	–
	20	4.33E-2	2.01	3.10E-4	3.06	9.49E-2	1.95	8.09E-3	1.93	1.79E-2	2.07	2.66E-4	3.04
	40	1.08E-2	2.00	3.79E-5	3.03	2.39E-2	1.99	2.05E-3	1.98	4.44E-3	2.01	3.29E-5	3.01
	80	2.70E-3	2.00	4.69E-6	3.02	6.00E-3	2.00	5.13E-4	2.00	1.11E-3	2.00	4.11E-6	3.00
2	10	2.32E-2	–	2.08E-4	–	3.19E-2	–	7.60E-4	–	1.44E-2	–	1.95E-4	–
	20	2.99E-3	2.95	1.29E-5	4.02	4.20E-3	2.92	4.96E-5	3.94	1.86E-3	2.95	1.22E-5	4.00
	40	3.77E-4	2.99	7.98E-7	4.01	5.32E-4	2.98	3.13E-6	3.98	2.34E-4	2.99	7.60E-7	4.00
	80	4.73E-5	3.00	4.97E-8	4.00	6.67E-5	3.00	1.96E-7	4.00	2.93E-5	3.00	4.75E-8	4.00

TABLE 11. History of convergence on polygonal meshes.

k	Mesh n	$\|\boldsymbol{q}-\boldsymbol{q}_h\|_{\mathcal{T}_h}$ error	order	$\|u-u_h^*\|_{\mathcal{T}_h}$ error	order	$\|\boldsymbol{q}-\boldsymbol{q}_h\|_{\mathcal{T}_h}$ error	order	$\|u-u_h^*\|_{\mathcal{T}_h}$ error	order	$\|\boldsymbol{q}-\boldsymbol{q}_h\|_{\mathcal{T}_h}$ error	order	$\|u-u_h^*\|_{\mathcal{T}_h}$ error	order
		LDG-H				LS				HHO			
1	10	1.55E-1	–	5.22E-3	–	1.16E-1	–	1.49E-3	–	1.16E-1	–	1.51E-3	–
	20	3.97E-2	1.96	1.03E-3	2.34	2.93E-2	1.98	1.87E-4	3.00	2.93E-2	1.98	1.88E-4	3.01
	40	1.06E-2	1.91	1.90E-4	2.43	7.51E-3	1.96	2.43E-5	2.95	7.51E-3	1.96	2.43E-5	2.95
	80	2.85E-3	1.89	3.47E-5	2.46	1.91E-3	1.98	3.12E-6	2.96	1.91E-3	1.98	3.12E-6	2.96
2	10	1.23E-2	–	1.68E-4	–	9.62E-3	–	1.03E-4	–	9.60E-3	–	1.03E-4	–
	20	1.46E-3	3.08	1.00E-5	4.07	1.17E-3	3.04	6.15E-6	4.06	1.17E-3	3.04	6.15E-6	4.06
	40	1.87E-4	2.97	8.02E-7	3.64	1.52E-4	2.95	4.00E-7	3.94	1.51E-4	2.95	4.00E-7	3.94
	80	2.44E-5	2.94	7.47E-8	3.42	1.95E-5	2.96	2.60E-8	3.95	1.95E-5	2.96	2.60E-8	3.94
		HDG-M				L-MIX				U-MIX			
1	10	1.11E-1	–	1.68E-3	–	2.53E-1	–	2.31E-2	–	7.10E-2	–	1.54E-3	–
	20	2.80E-2	1.98	2.08E-4	3.02	6.54E-2	1.95	6.28E-3	1.88	1.72E-2	2.05	1.93E-4	3.00
	40	7.28E-3	1.94	2.70E-5	2.95	1.72E-2	1.93	1.65E-3	1.93	4.46E-3	1.94	2.51E-5	2.94
	80	1.87E-3	1.96	3.46E-6	2.96	4.41E-3	1.96	4.22E-4	1.96	1.16E-3	1.94	3.25E-6	2.95
2	10	9.25E-3	–	1.04E-4	–	1.40E-2	–	3.50E-4	–	7.28E-3	–	1.06E-4	–
	20	1.14E-3	3.01	6.17E-6	4.08	1.81E-3	2.95	2.26E-5	3.95	8.19E-4	3.15	6.21E-6	4.10
	40	1.50E-4	2.93	4.07E-7	3.92	2.33E-4	2.96	1.55E-6	3.87	1.05E-4	2.96	4.12E-7	3.91
	80	1.96E-5	2.93	2.66E-8	3.93	3.02E-5	2.95	1.03E-7	3.92	1.39E-5	2.93	2.70E-8	3.93

On the other hand, the errors in u_h^* for HDG-M, LS, HHO, and U-MIX are about the same, those for LDG-H slightly bigger, and those for L-MIX even bigger than those for LDG-H.

Table 11 presents the history of convergence for the six methods on polygonal meshes for $k = 1$ and $k = 2$. Again, we observe slightly better convergence rates than predicted by the theory for LDG-H, and expected convergence rates for the other five methods. When $k = 1$, we have about second-order convergence rate in $\boldsymbol{q}_h$ for all the methods, and about 2.5 convergence rate in u_h^* for LDG-H, second-order convergence rate for L-MIX, and third-order convergence for the other four methods. When $k = 2$, we have about third-order convergence rate in $\boldsymbol{q}_h$ for all the methods, and about 3.4 convergence rate in u_h^* for LDG-H and fourth-order convergence for the other five the methods. This time, L-MIX produces the biggest errors in $\boldsymbol{q}_h$. For the other five methods, the errors in $\boldsymbol{q}_h$ for HDG-M, LS, and HHO are about the same, those for LDG-H are slightly bigger, and those for U-MIX slightly smaller. On the other hand, the errors in u_h^* for HDG-M, LS, HHO, and U-MIX are about the same, those for LDG-H slightly bigger, and those for L-MIX are even bigger than those of LDG-H. However, when we refine the mesh once more, the the errors in u_h^* for L-MIX with $k = 2$ are smaller than those for LDG-H.

6. Concluding remarks

We have applied the theory of M-decomposition to systematically construct HDG and their sandwiching mixed methods on polygonal meshes. We have also numerically compared our superconvergent HDG and their sandwiching mixed methods with other superconvergent LS-like and HHO-like HDG methods and have verified, in a very simple model problem, that the expected orders of convergence are achieved and that all these methods produce similar errors with similar computational effort for solving the global problem. The corresponding construction in three-space dimensions is carried out in Part III, [14], of this series. A more thorough numerical comparison between the several methods considered here, as well as the automatic computation of the spaces $\delta \boldsymbol{V}_{\rm fillM}$ and $\delta \boldsymbol{V}_{\rm fillW}$ are the subject of ongoing work.

References

[1] T. Arbogast and H. Xiao, Two-level mortar domain decomposition mortar preconditioners for heterogeneous elliptic problems. *Comput. Methods Appl. Mech. Engrg.* **292** (2015) 221–242.

[2] D.N. Arnold, D. Boffi and R.S. Falk, Quadrilateral $H(\text{div})$ finite elements. *SIAM J. Numer. Anal.* **42** (2005) 2429–2451 (electronic).

[3] P. Bastian and B. Riviere, Superconvergence and $H(\text{div})$ projection for discontinuous Galerkin methods. *Int. J. Numer. Meth. Fluids* **42** (2003) 1043–1057.

[4] L. Beirao da Veiga, F. Brezzi, A. Cangiani, G. Manzini, L.D. Marini, and A. Russo, Basic principles of Virtual Element Methods. *Math. Models Methods. Appl. Sci.* **23** (2013) 199–214.

[5] L. Beirao da Veiga, F. Brezzi, L.D. Marini and A. Russo, H(div) and H(curl)-conforming VEM. *Numer. Math.* **133** (2016) 303–332.

[6] D. Boffi, F. Brezzi and M. Fortin, *Mixed Finite Element Methods and Applications*. Springer-Verlag, New York (2013).

[7] F. Brezzi, J. Douglas, Jr. and L.D. Marini, Two families of mixed finite elements for second order elliptic problems. *Numer. Math.* **47** (1985) 217–235.

[8] F. Brezzi, J. Douglas Jr, M. Fortin and L.D. Marini, Efficient rectangular mixed finite elements in two and three space variables. *ESAIM: M2AN* **21** (1987) 581–604.

[9] F. Brezzi, R.S. Falk and L.D. Marini, Basic principles of mixed Virtual Element Methods. *ESAIM: M2AN* **48** (2014) 1227–1240.

[10] P. Castillo, B. Cockburn, I. Perugia and D. Schotzau, An a priori error analysis of the local discontinuous Galerkin method for elliptic problems. *SIAM J. Numer. Anal.* **38** (2000) 1676–1706.

[11] Y. Chen and B. Cockburn, Analysis of variable-degree HDG methods for convection-diffusion equations. Part I: General nonconforming meshes. *IMA J. Numer. Anal.* **32** (2012) 1267–1293.

[12] Y. Chen and B. Cockburn, Analysis of variable-degree HDG methods for convection-diffusion equations. Part II: Semimatching nonconforming meshes. *Math. Comput.* **83** (2014) 87–111.

[13] B. Cockburn, Static condensation, hybridization and the devising of the HGD methods, in LNCSE Series, Building Bridges: Connections and Challenges in Modern Approaches to Numerical Partial Differential Equations, edited by G.R. Barrenechea, F. Brezzi, A. Cagiani and E.H. Georgoulis. Durham Symposium, London Mathematical Society, Durham, UK (2014) 7–16.

[14] B. Cockburn and G. Fu, Superconvergence by M-decompositions. Part III: Construction of three-dimensional finite elements. To appear in *ESAIM: M2AN* Doi:10.1051/m2an/2016023 (2016).

[15] B. Cockburn and W. Qiu, Commuting diagrams for the TNT elements on cubes. *Math. Comput.* **83** (2014) 603–633.

[16] B. Cockburn, G. Kanschat and D. Schötzau, A locally conservative LDG method for the incompressible Navier-Stokes equations. *Math. Comput.* **74** (2005) 1067–1095.

[17] B. Cockburn, J. Gopalakrishnan and R. Lazarov, Unified hybridization of discontinuous Galerkin, mixed and continuous Galerkin methods for second order elliptic problems. *SIAM J. Numer. Anal.* **47** (2009) 1319–1365.

[18] B. Cockburn, J. Gopalakrishnan and F.-J. Sayas, A projection-based error analysis of HDG methods. *Math. Comput.* **79** (2010) 1351–1367.

[19] B. Cockburn, W. Qiu and K. Shi, Conditions for superconvergence of HDG methods for second-order elliptic problems. *Math. Comput.* **81** (2012) 1327–1353.

[20] B. Cockburn, G. Fu and F.-J. Sayas, Superconvergence by M-decompositions. Part I: General theory for HDG methods for diffusion. To appear in *Math. Comput.* (2016).

[21] B. Cockburn, D. DiPietro and A. Ern, Bridging the Hybrid High-Order and Hybridizable Discontinuous Galerkin Methods. *ESAIM: M2AM* **50** (2016) 635–650.

[22] D.A. Di. Pietro and A. Ern and S. Lemaire, An arbitrary-order and compact-stencil discretization of diffusion on general meshes based on local reconstruction operators. *Comput. Methods Appl. Math.* **14** (2014) 461–472.

[23] D.A. Di Pietro and A. Ern, A hybrid high-order locking-free method for linear elasticity on general meshes, *Comput. Methods Appl. Mech. Engrg.* **283** (2015) 1–21.

[24] A. Ern, S. Nicaise and M. Vohralík, An accurate $\mathbf{H}(\text{div})$ flux reconstruction for discontinuous Galerkin approximations of elliptic problems. *C. R. Math. Acad. Sci. Paris* **345** (2007) 709–712.

[25] A. Gillette, A. Rand and C. Bajaj, Error estimates for generalized barycentric interpolation. *Adv. Comput. Math.* **37** (2012) 417–439.

[26] Y. Kuznetsov and S. Repin, New mixed finite element method on polygonal and polyhedral meshes. *Russ. J. Numer. Anal. Math. Model.* **18** (2003) 261–278.

[27] Y. Kuznetsov and S. Repin, Convergence analysis and error estimates for mixed finite element method on distorted meshes. *J. Numer. Math.* **13** (2005) 33–51.

[28] C. Lehrenfeld, *Hybrid Discontinuous Galerkin methods for solving incompressible flow problems*. Diploma Thesis. Rheinisch-Westfälischen Technischen Hochschule, Aachen (2010).

[29] G. Manzini, A. Russo and N. Sukumar, New perspectives on polygonal and polyhedral finite element methods. *Math. Models Methods Appl. Sci.* **24** (2014) 1665–1699.

[30] I. Oikawa, A hybridized discontinuous Galerkin method with reduced stabilization. *J. Sci. Comput.* **65** (2015) 327–340.

[31] P.A. Raviart and J.M. Thomas, A mixed finite element method for second order elliptic problems, in Mathematical Aspects of Finite Element Method, edited by I. Galligani and E. Magenes. Vol. 606 of *Lect. Notes Math.* Springer-Verlag, New York (1977) 292–315.

[32] A. Sboui, J. Jaffré and J. Roberts, A composite mixed finite element for hexahedral grids. *SIAM J. Sci. Comput.* **31** (2009) 2623–2645.

[33] M. Vohralík and B. Wohlmuth Mixed finite element methods: implementation with one unknown per element, local flux expressions, positivity, polygonal meshes, and relations to other methods. *Math. Models Methods Appl. Sci.* **23** (2013) 803–838.

[34] J. Warren, Barycentric coordinates for convex polytopes. *Adv. Comput. Math.* **6** (1996) 97–108.